Journal of Umm Al-Qura University for Engineering and Architecture
https://doi.org/10.1007/s43995-025-00224-y

ORIGINAL ARTICLE

Buckling behavior of thin-walled cylindrical shell structure under axial compression: A study of imperfection parameters with FE approach

Aryanda Rakhmad Maharditya[1] · Ben Ganendra[1,2] · Indri Yaningsih[1] · Aditya Rio Prabowo[1] · Sören Ehlers[3,4] · Moritz Braun[3] · Quang Thang Do[5] · Wibowo Wibowo[1] · Teguh Muttaqie[6] · Iwan Istanto[1] · Rahman Wijaya[1]

Received: 26 May 2025 / Accepted: 6 September 2025

Abstract
Cylindrical shell structures are widely used in engineering applications, particularly in ships and aircraft, due to their high strength-to-weight ratio and efficiency in resisting compressive loads. However, these structures are susceptible to failure through buckling, especially when imperfections such as load eccentricity, thickness variation, and initial geometric deviations are present. This study examines the structural response of thin-walled cylindrical shells subjected to axial compression, taking into account various imperfections. A finite element (FE) approach using ABAQUS software was employed and validated against previous experimental data. A parametric study was conducted using varying load eccentricity, initial geometric imperfections, and longitudinal thickness. The results show that load eccentricity significantly reduces the ultimate load and shifts the location of deformation. Both geometric and thickness imperfections also affect structural strength and the location of buckling. These findings enhance the reliability and safety of cylindrical shell designs in engineering applications.

Keywords Finite element method · Geometric imperfection · Cylindrical shell · Ultimate strength · Buckling behavior

1 Introduction

Thin-walled structures are engineering components distinguished by their wall thickness being much smaller than their dimensions. This geometry enables them to bear loads while efficiently minimizing material usage. Examples of thin-walled structures include plates, shells, beams, and trusses, which are designed to distribute loads effectively, often resulting in lightweight construction. The analysis and design of thin-walled structures require a deep understanding of material behavior and structural mechanics, as their slenderness can make them susceptible to some mechanical behaviors, such as buckling [1].

Cylindrical shells are widely used in ship structures due to their strength-to-weight ratio, structural efficiency, and ability to withstand various loads and pressures. These shells are inherently stable because of their curved geometry, which evenly distributes stresses and resists buckling under compression or bending forces [2]. This makes it particularly effective in handling the forces experienced by ships, such as wave impacts, cargo loads, and water pressure [3]. Additionally, cylindrical shells are economical in terms of material usage, as their thin-walled construction achieves high strength while minimizing weight. This is critical for enhancing buoyancy and reducing fuel consumption. Moreover, cylindrical shells are versatile. They can be adapted for different ship types and applications, such as submarines or tankers, where pressure resistance is essential.

✉ Aditya Rio Prabowo
aditya@ft.uns.ac.id

1 Department of Mechanical Engineering, Universitas Sebelas Maret (UNS), Surakarta, Indonesia

2 Department of Civil Engineering, Ghent University, Ghent, Belgium

3 Institute for Maritime Energy Systems, German Aerospace Center, Geesthacht, Germany

4 Institute for Ship Structural Design and Analysis, Hamburg University of Technology, Hamburg, Germany

5 Department of Naval Architecture and Ocean Engineering, Nha Trang University, Nha Trang, Vietnam

6 Research Center for Hydrodynamics Technology, National Research and Innovation Agency (BRIN), Surabaya, Indonesia

Published online: 07 October 2025

The cylindrical shell structure has a good ability to withstand even compressive forces, which is influenced by its symmetrical geometry and structural rigidity, which allows for more effective load distribution over the entire surface of the structure [4]. In the case of axial forces, the load applied along the vertical axis of the cylinder is also evenly distributed along the surface. This structure is different from other structures, which tend to have a more uneven load distribution [5]. In addition to having a good ability to withstand even compressive force, the cylindrical shell structure also has good structural efficiency [6].

Buckling analysis of the structure of a cylindrical shell was first performed in 1933 by Eugene E. Lundquist [7]. This research continues to be developed today due to its widespread use in various engineering fields, including airplanes, submarines, and storage tanks [8]. Buckling is one of the primary failure factors in cylindrical shell structures; accurately predicting their response is crucial for minimizing the risk of failure. However, predicting failure due to buckling is not always as straightforward as it seems. Geometric imperfections, such as minor deviations from the ideal shape of the shell [9], as well as load eccentricity, can significantly affect the response of the structure to axial loads [10]. Previous research by [11] It has been shown that minor imperfections in the shell structure can reduce the critical load capacity.

Huang et al. demonstrated that geometric imperfections and temperature-dependent material properties can significantly diminish the buckling resistance of functionally graded cylindrical shells [12]. Similarly, Himayat Ullah's comparative work using analytical, numerical, and semi-empirical models revealed that theoretical predictions often overestimate buckling loads by 15%–50%, primarily due to the neglect of imperfections [13]. Additional studies by Chulin Yu et al. have examined the role of welding residual stresses, showing their substantial influence on plastic buckling behavior and deformation characteristics [14].

Cao et al. developed a unified analytical model that accounted for thickness imperfections using Fourier series expansion and perturbation methods. They observed buckling load reductions of up to 34.1% in specific configurations [15]. Ifayefunmi's experiments on MIG-welded mild steel cylinders further confirmed that both elastic and plastic buckling modes are dependent on wall thickness and radius-to-thickness ratios [16]. Likewise, research by Zhiping Chen et al. emphasized that external factors such as differential settlement and internal hydrostatic pressure significantly affect buckling capacity [17].

Recent investigations by Tu et al. [18] and Badamchi et al. [11] have explored the effects of eccentric axial loads and combined axial-external pressures, respectively. These studies confirmed the nonlinear interaction between loading conditions and buckling capacity, underlining the importance of parametric analysis in improving prediction accuracy and optimizing structural safety.

This paper investigates the compressive strength of cylindrical shell structures subjected to compressive load. The model employed in this study is based on the experimental framework proposed by [11], whose experimental results served as a reference to validate the numerical solution in terms of ultimate load in the present study, in which the Riks solver is utilized, replacing the general static solver used in [11]. Several other research [19, 20] utilized a similar framework in validating the numerical results by comparing them with their test counterparts for various purposes, such as enhancing the structural safety. A parametric study is conducted to investigate the relationship between compressive strength and imperfections, including initial geometric imperfections, load eccentricity, and thickness imperfections, in cylindrical shells.

2 Governing equation in pipe compression

2.1 Buckling load equation

The Buckling Load Factor (BLF) indicates the safety margin against buckling failure in structures subjected to compressive loads. It is calculated as the ratio of the critical buckling load (P_{cr}) to the applied load $P_{applied}$, defined as Eq. 1.

$$\text{BLF} = \frac{P_{cr}}{P_{applied}} \tag{1}$$

where P_{cr} is the critical load at which buckling occurs. The critical axial load at buckling for a thin-walled pipe can be defined using shell theory as Eq. 1.

$$P_{cr} = \frac{2\pi E t^2}{\sqrt{3(1-v^2)}} \tag{2}$$

P_{cr} = Critical load.
E = Young's modulus,
v = Poisson's ratio.
t = Wall thickness.

This equation assumes the pipe is thin-walled, the load is applied axially and uniformly. Practical considerations like geometric imperfections and material variability often lower the actual buckling load, necessitating safety factors [21]. $P_{applied}$ is the load currently acting on the structure. A BLF greater than 1 indicates that the applied loads are below the critical threshold, suggesting that buckling is not expected.

2.2 Safety factor

Safety factors are employed to assess the integrity of components or structures [22] and can be broadly defined as the ratio of the maximum load that a structure can sustain to the load for which it is designed. The primary objective of a safety factor is to protect the completed structure from damage or failure resulting from applied loads or conditions that may exceed or be more severe than those that a proficient designer can reasonably anticipate [23]. The safety factor can be expressed as Eq. 2.

$$SF = \frac{P_{cr}}{P_{applied}} \tag{3}$$

where P_{cr} is the critical load, $P_{applied}$ is the applied load in the structure. Safety factors are established for thin-walled pipes subjected to axial compression by analyzing critical buckling loads, material properties, and geometric considerations.

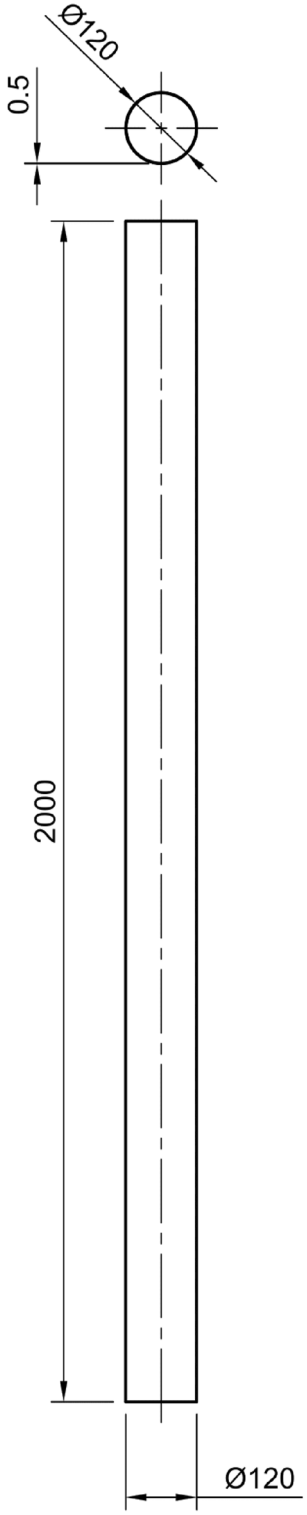

Fig. 1 DT240-F model

3 Validation methodology

3.1 Geometrical model

The diameter-to-wall-thickness ratio is a crucial parameter in thin-walled structures. Many researchers have investigated that the D/t ratio will influence the buckling behavior and the critical compressive strain [24–26]. In this numerical analysis study, a cylindrical shell pipe geometry was employed. The variation in geometry is characterized by the diameter-to-thickness ratio (D/t). Three geometry variations were used in this research: DT240-F (Fig. 1), DT200-F (Fig. 2), and DT171-F (Fig. 3), where F is the axial compression applied to the pipe.

3.2 Mesh convergence study

Mesh convergence is performed to obtain a mesh size range that yields stable simulation results. Meshes with a large size will give inaccurate results. At the same time, meshes that are too small will result in very long computational times without significantly improving the accuracy of the results. Mesh convergence is helpful to ensure that the FEM model can provide relevant results [27]. This study needs to be conducted before proceeding to parametric studies. To this end, the mesh size was reduced from the smallest to the largest.

3.3 Benchmarking study

3.3.1 Profile of the testing reference

The previous research conducted by Badamchi and Showkati [11] began with an experimental analysis and was validated by a numerical analysis. The experimental study

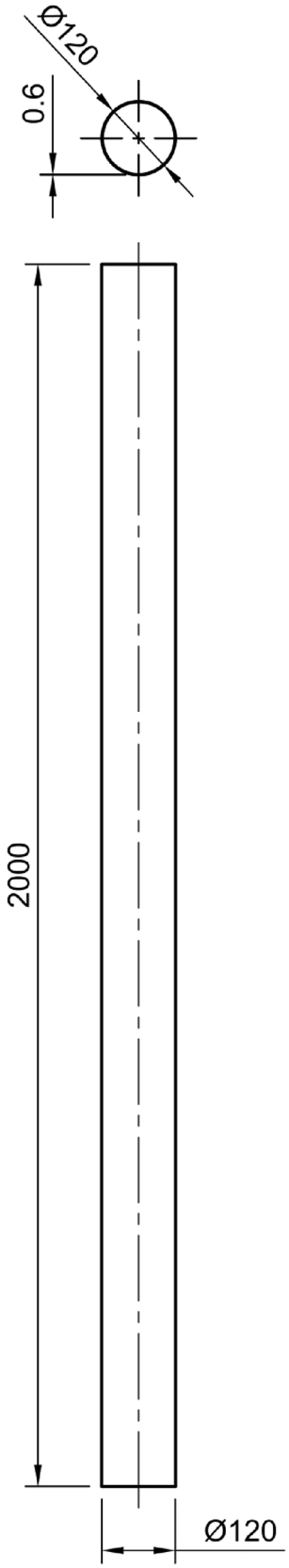

Fig. 2 DT200-F model

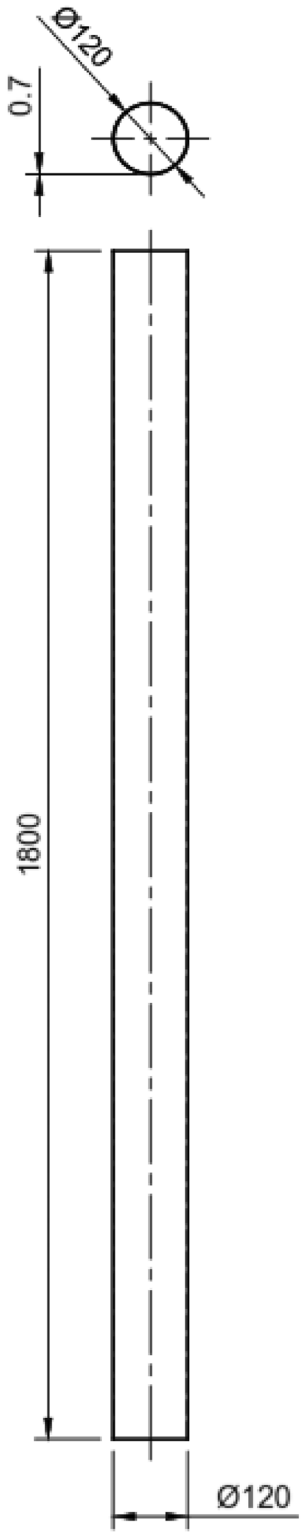

Fig. 3 DT171-F model

began with manufacturing a rectangular sheet and then rolling it along its length. The sheet was welded using an argon weld to form a single piece of pipe. Due to manufacturing limitations, the pipe is divided into two parts with a

maximum length of L = 1000 mm. The two individual pipes are circumferentially welded together to form a single, longer pipe, as shown in Fig. 4. The welded sides were covered with paper tape, the entire external pipe was painted, and then meshed using drawn lines, as shown in Fig. 5.

Figure 6 shows the schematic of the experimental setup. The rig used in this research had one sliding end and one fixed end on the other side. Hydraulic jacks were used to apply axial compression, allowing for the axial shortening of the pipes. A variation in the diameter-to-thickness ratio (D/t) was employed; three geometries were examined, namely DT 240-F, DT 200-F, and DT 171-F. The dimensions of each geometry are detailed in Table 1.

After the experiment, numerical analysis was conducted to validate the experimental results. Validation is carried out by ensuring the methods used are equal and minimizing the error in the results between numerical analysis and experimental results.

3.3.2 Benchmarking setup

The setup in the numerical simulation was adopted from the actual setup. ABAQUS software was used in the numerical analysis in this study. Pipe geometry is defined as a deformable body. To obtain the loading and buckling mode results in this study and to determine the compressive strength of the model, which is evaluated based on the load proportional factor. A linear eigenvalue buckling analysis is applied, using the step procedure, namely Static Riks. In the interaction module, the two ends of the pipe are defined as a rigid body, and the region type is defined as a tie. Steel material was used in this study, and the material properties were detailed in Table 2.

The numerical analysis was performed by applying axial loads from one end. An axial compression force (N) was applied to the shell quasistatically until the critical load was reached. The loading scheme is illustrated in Fig. 7, where the axial load is applied.

The geometry has two boundary conditions, a moving end and a fixed end, which are defined as displacement/rotation, as shown in Fig. 8. The displacement was restricted at the X and Z axes; the configuration is detailed in Table 3.

Based on the experimental analysis, two imperfections were identified during the study and subsequently incorporated into the numerical analysis. The first imperfection is loading eccentricity, which happened because, in reality, the applied axial compression may act at an eccentric position. The schematic of the applied force is shown in Fig. 9. The load eccentric imperfection in the numerical analysis was used by moving the applied load position by a distance of e (e = 0.005D = 0.6 mm).

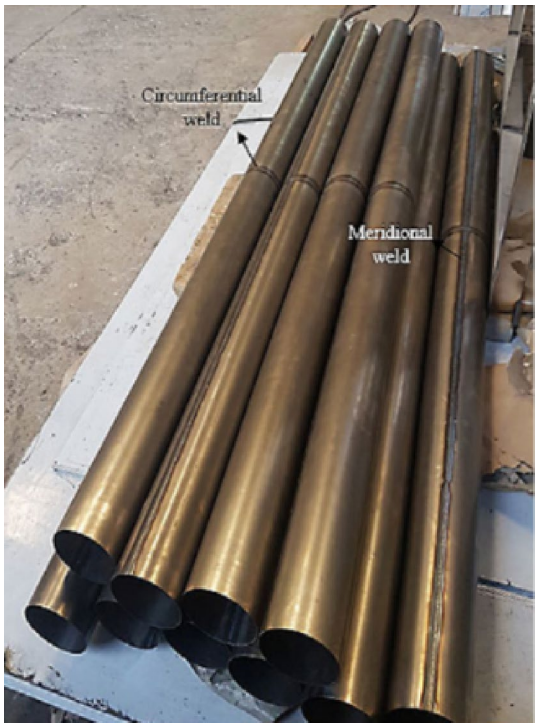

Fig. 4 Pipe after manufacturing [11]

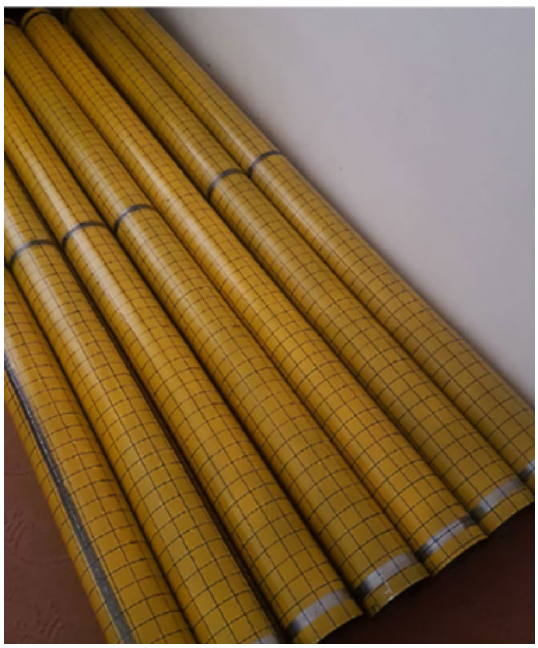

Fig. 5 Mesh drawn lines on the pipe [11]

The research conducted by Kainat et al. revealed that the wall thickness of pipe segments varied in both the peripheral and longitudinal directions [9]. The thickness of the pipe changed in the longitudinal direction defined by Eq. 3.

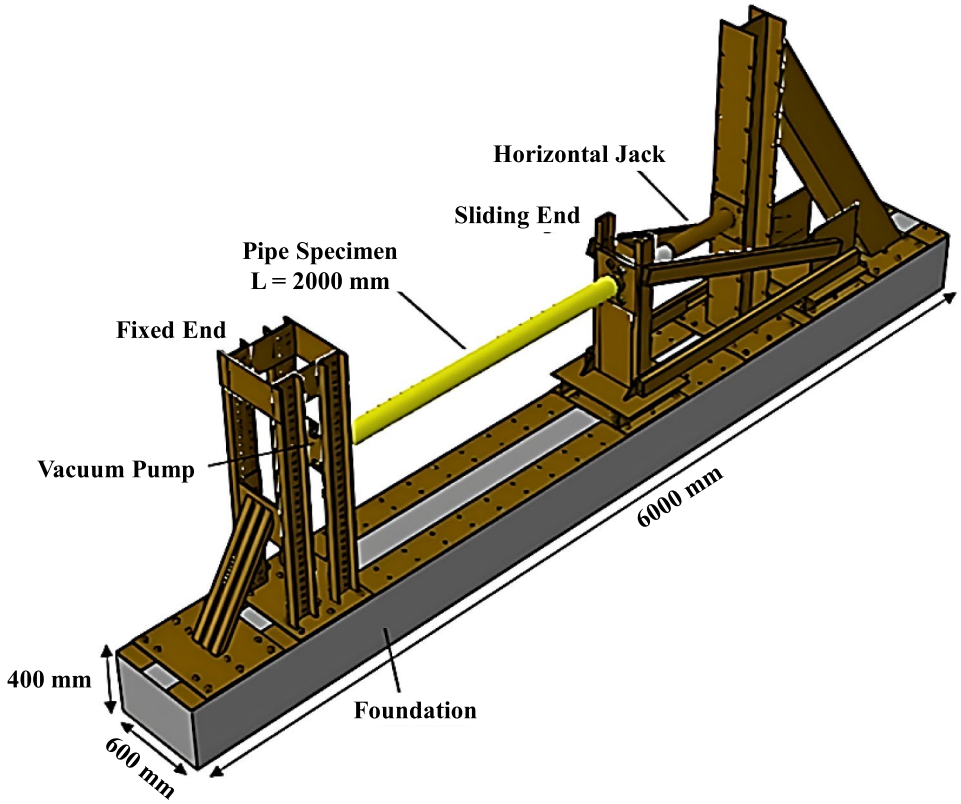

Fig. 6 Schematic of experimental setup [11]

Table 1 Geometry of the test model

Specimen label	L (mm)	D (mm)	t (mm)
DT240-F	2000	120	0.5
DT200-F	2000	120	0.6
DT171-F	1800	120	0.7

Table 2 Material properties of the designed pipes

Properties	Values
Density, $\rho(\mathrm{kg/m^3})$	7850
Young's Modulus, E (MPa)	200,000
Yield stress, A (MPa)	180
Poisson's ratio	0.3

$$t_z = \alpha.t + \frac{1-\alpha}{2} \times \cos\frac{\beta\pi z}{L} + C \tag{4}$$

where the wall thickness along the length of the pipe is represented by t_z, while z denotes the distance from a specified cross-section to the defined coordinate system positioned at one end of the pipe. The parameters α, β, and C are constants that must be determined (as shown in Table 4). The variation in thickness along the pipe, considered an imperfection, is illustrated in Fig. 10 using Eq. 3.

To input the mapped thickness along the pipe into the ABAQUS software, MATLAB was used to generate the coordinates of the pipe's circle. The programming code is shown in Fig. 11. Using analytical field distribution attributes in ABAQUS, the generated circle coordinate and the varied thickness were input simultaneously.

4 Methodology of parametric study

The benchmarking setup has been completed, ensuring the precise prediction of the compression behavior of cylindrical shells. The same numerical simulation setup used in the benchmarking process is adopted for the parametric study, which aims to evaluate the influence of initial geometric imperfection, thickness imperfection, and load eccentricity.

4.1 Eccentricity of load

Eccentric loading in thin-walled cylindrical shells under axial compression refers to a force applied off-center from the cylinder's axis, creating a distance, or eccentricity (e), between the load's line of action and the axis, as shown in Fig. 12. This deviation induces compressive stress, significantly affecting the cylinder's structural integrity. Unlike concentric loads, which apply force through the center of gravity to achieve uniform stress distribution, eccentric loads cause uneven stress distribution. Load eccentricity is crucial in determining the buckling response of pipelines and in engineering design to ensure structures can withstand

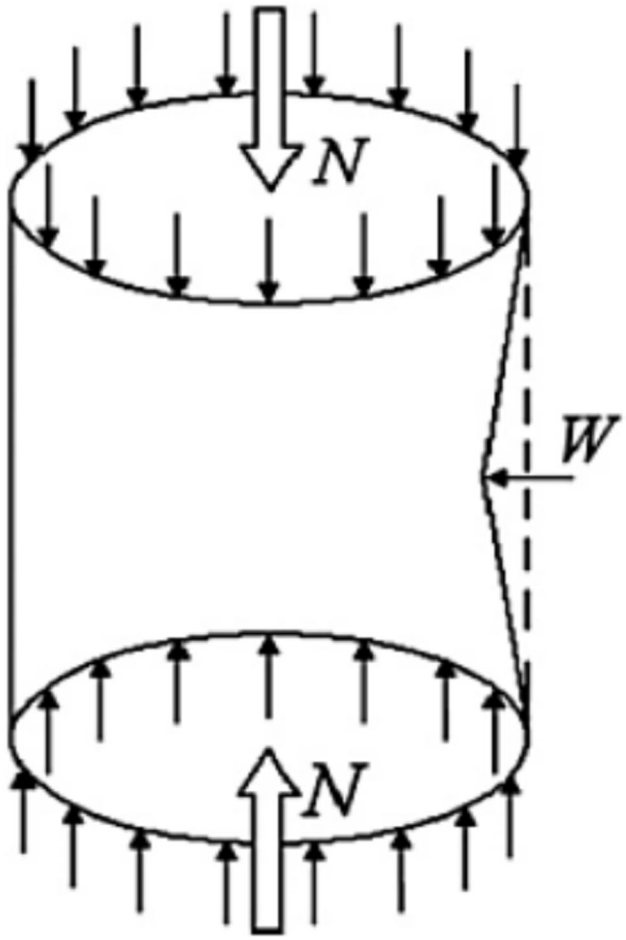

Fig. 7 Loading scheme on the cylindrical shell [28]

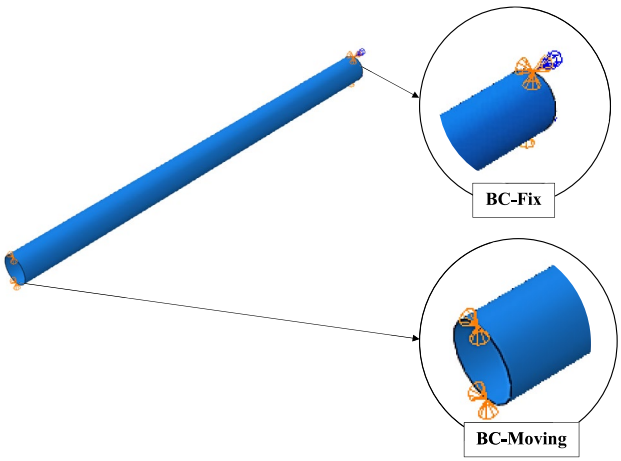

Fig. 8 Applied boundary condition on the model

Table 3 Boundary condition for finite element configuration

Name	Configuration
BC-Fix	$U_1 = 0$
	$U_2 = 0$
	$U_3 = 0$
	$UR_1 = 0$
BC-Moving	$U_1 = 0$
	$U_2 = 0$

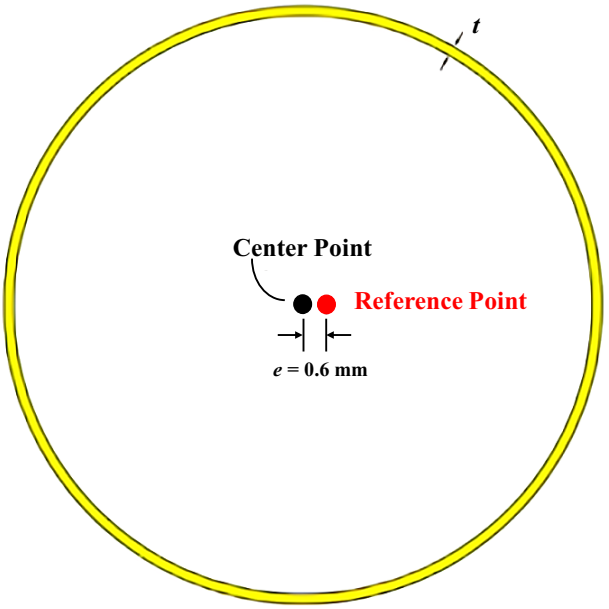

Fig. 9 Position of applied axial compression [11]

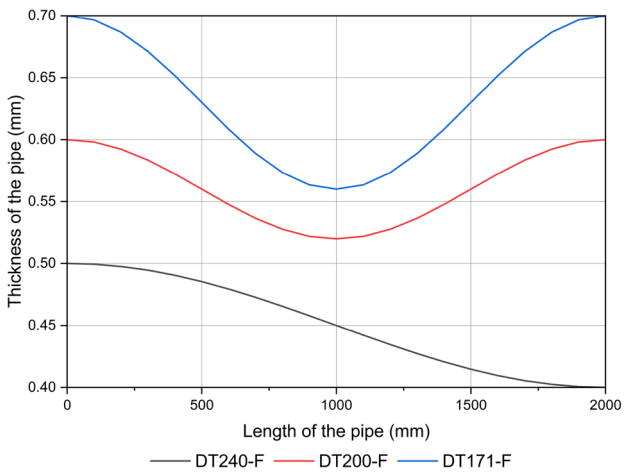

Fig. 10 Thickness variation along the pipe

Table 4 Input parameter for Eq. 3

Specimens label	α	β	$C = t_{specimens} - t_{(z-0)}$
DT240-F	90%	1	0
DT200-F	92%	2	0.008
DT171-F	86%	2	0.028

Fig. 11 MATLAB code to generate circle coordinates

```
% Example usage:
radius = 60;      % Define the radius of the circle
num_points = 346; % Define the number of points along the circumference

% Generate the circle coordinates
circle_coords = generate_circle_coordinates(radius, num_points);

% Display the coordinates
disp('X, Y coordinates along the circumference of the circle:');
disp(circle_coords);

% Plot the circle
figure;
plot(circle_coords(:, 1), circle_coords(:, 2), 'bo-');
axis equal;
title('Circle Coordinates');
xlabel('X');
ylabel('Y');
```

Fig. 12 Schematic of the pipe under eccentric loading [18]

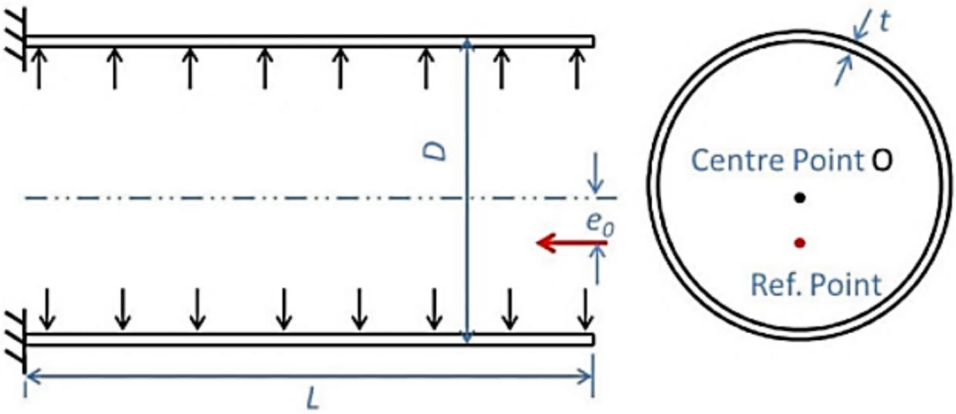

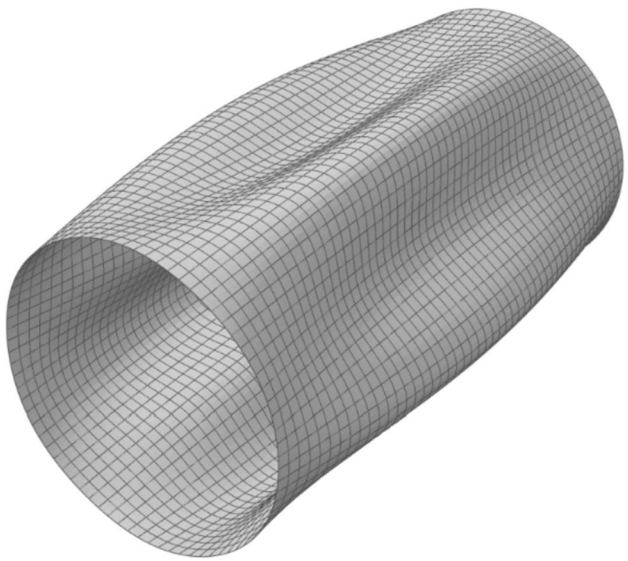

Fig. 13 Initial geometric imperfection scheme

real-world conditions, such as wind, seismic activity, or uneven settlement [29].

The geometries DT240-F, DT200-F, and DT171-F were used in this parametric study. The variation of the eccentric load will be applied on the center along the X-axis; the magnitude variation can be defined as Eq. 4.

$$Eccentric\ ratio = e \times D \tag{5}$$

E = Eccentric magnitude.

D = Diameter of the pipe.

4.2 Initial geometric imperfection

Initial geometric imperfections in thin-walled cylindrical shells under axial compression refer to deviations of the shell's initial geometry from its perfect ideal shape, as shown in the scheme of initial geometric imperfection in Fig. 13. These imperfections generally arise from manufacturing processes and significantly influence the structure's load-carrying capacity, stiffness, and post-buckling behavior. Incorporating these imperfections into structural design

Table 5 Alpha variation of thickness imperfection

Thickness number	Thickness imperfection	
	Alpha	Beta
Thickness_1	0.9	1
Thickness_2	0.88	1
Thickness_3	0.86	1

Table 6 Beta variation of thickness imperfection

Thickness number	Thickness imperfection	
	Alpha	Beta
Thickness_5	0.9	1
Thickness_6	0.9	2
Thickness_7	0.9	4

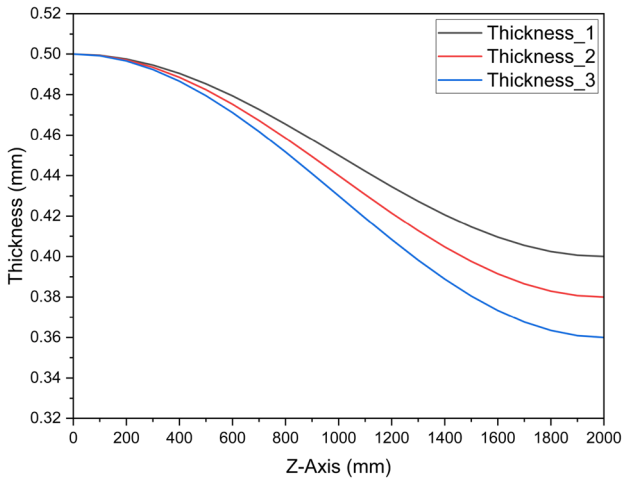

Fig. 14 Thickness variation along the pipe (alpha variation)

and analysis is crucial for accurately predicting buckling loads and ensuring structural integrity.

The geometric will only use DT240-F and DT171-F; the imperfection is defined using buckle analysis, which slightly varies the pipe diameter. An elastic linear eigenvalue buckling analysis was performed, and the first buckling mode amplitudes were scaled by a factor of $Initial\ imperfection = magnitude\ .\ thickness$, were applied as imperfections in the software, using the following direction: *IMPERFECTION, FILE=(name of input file in buckling analysis), STEP1=1 1, 0.6.

4.3 Longitudinal thickness imperfection

Longitudinal thickness imperfection in thin-walled cylindrical shells refers to variations or deviations in the shell's thickness along its length, which can significantly influence its structural behavior, particularly under axial compression. These imperfections, even if small (on the order of wall thickness), can substantially reduce the buckling load, making the cylinder sensitive to buckling conditions. The thickness variation can be defined from (see Eq. 8). In this

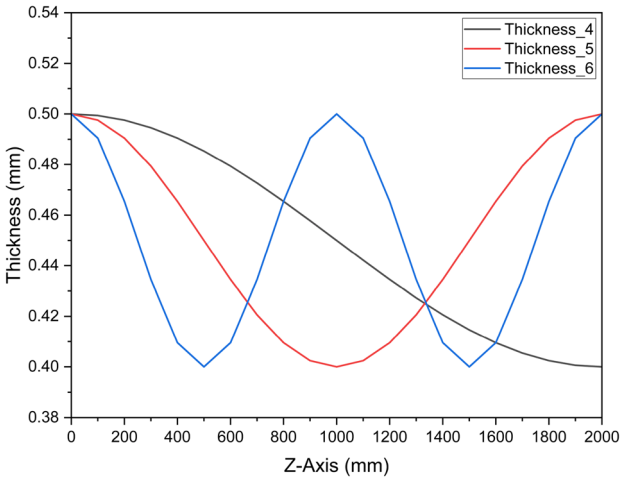

Fig. 15 Thickness variation along the pipe (beta variation)

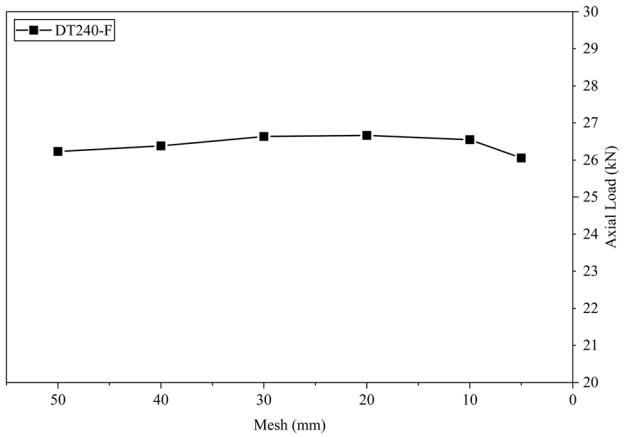

Fig. 16 Mesh convergence results of DT240-F

research, the simulation will only use the DT240-F geometry, and the thickness will be separated into two variations: the first will vary alpha, and the second will vary beta. The variation is evident in Tables 5 and 6 and illustrated in Figs. 14 and 15.

5 Verification results

5.1 Mesh convergence

Mesh convergence studies were conducted to determine the optimal mesh size that strikes a balance between accuracy and computational efficiency. As shown in Figs. 16, 17, 18, the axial loads between the present and previous configurations converge with a relatively stable prediction, suggesting minimal sensitivity to mesh refinement beyond a certain threshold. Based on the accuracy and runtime trade-off, a mesh size of 10 mm was selected for all further simulations. Visual comparisons in Figs. 19, 20, 21, 22, 23, 24

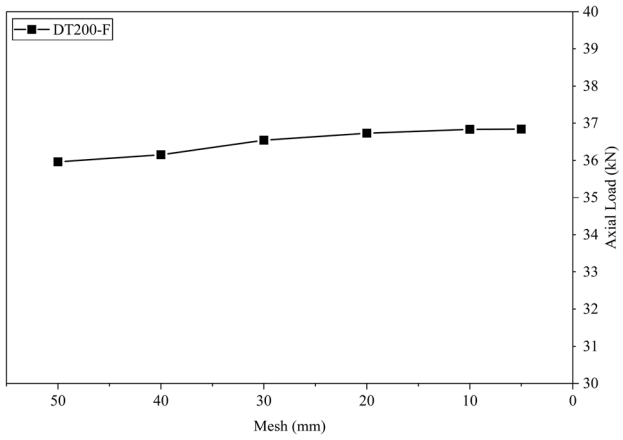

Fig. 17 Mesh convergence results of DT200-F

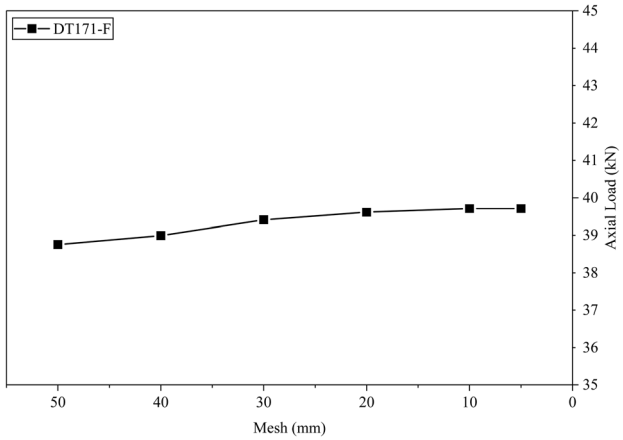

Fig. 18 Mesh convergence results of DT171-F

confirm that the deformation shapes are consistent with those reported in prior work, supporting the validity of this mesh selection.

5.2 Benchmarking study

In this study, the prediction of compressive strength obtained from the experimental data of a previous researcher [11] and the axial load will serve as a reference for conducting the numerical analysis. By comparing the results with those from the previous Finite Element Analysis (FEA) configuration [11], the ultimate load results for the three geometries are presented in Table 7. The deformation shape of the geometries is also considered in this study, as shown in Figs. 19, 20, 21, 22, 23, 24, where mesh 10 is used in every geometry. The deformation shape resembles that of the previous research.

For the DT240-F specimen, both the previous and current numerical results exhibit a similar deformation pattern, concentrated near the tube ends, confirming that the failure mode remains consistent. The difference lies in the way the deformation is captured. In the present result, the stress distribution is more localized, and the buckling folds appear sharper, whereas in the previous result, the distribution is more spread out, and the folds look smoother. The sharper folds in the present result resemble more closely the deformation observed in the experimental findings.

For the DT200-F specimen, the deformation mode is also consistent in both studies, occurring at the mid-span of the tube. However, the wave-shaped buckling is more visible in the present result, with more precise and more distinct lines compared to the smoother pattern in the previous result. This indicates that the present analysis captures the wave

Fig. 19 Numerical analysis result of DT240-F (previous study)

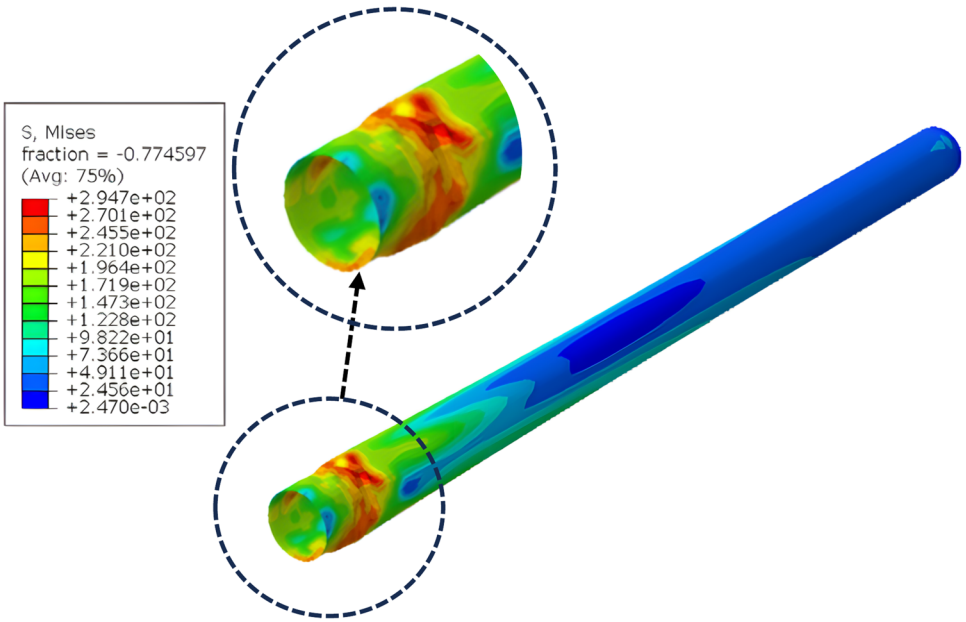

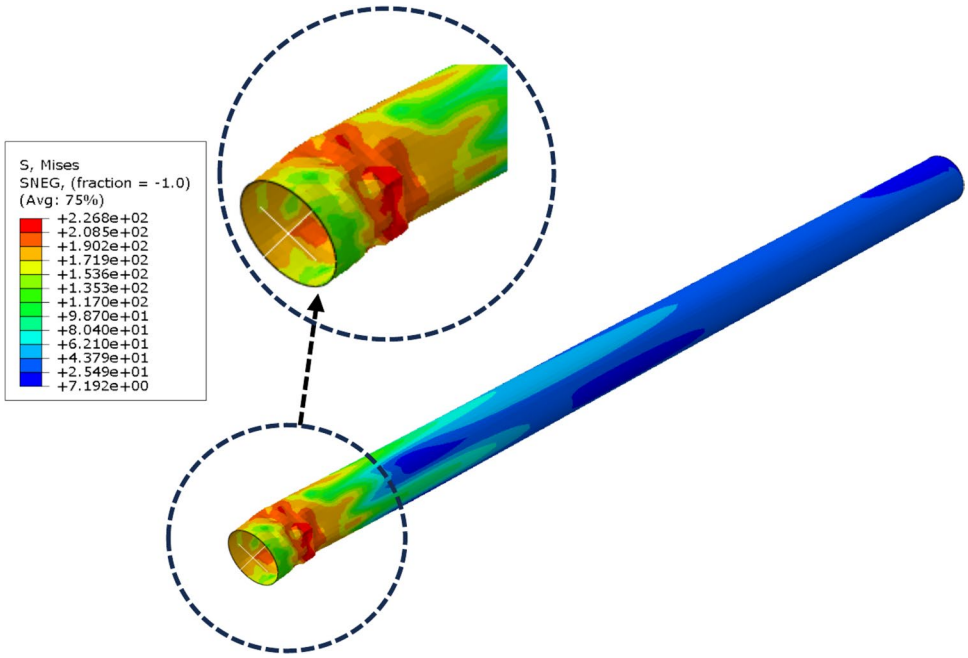

Fig. 20 Numerical analysis result of DT240-F (present study)

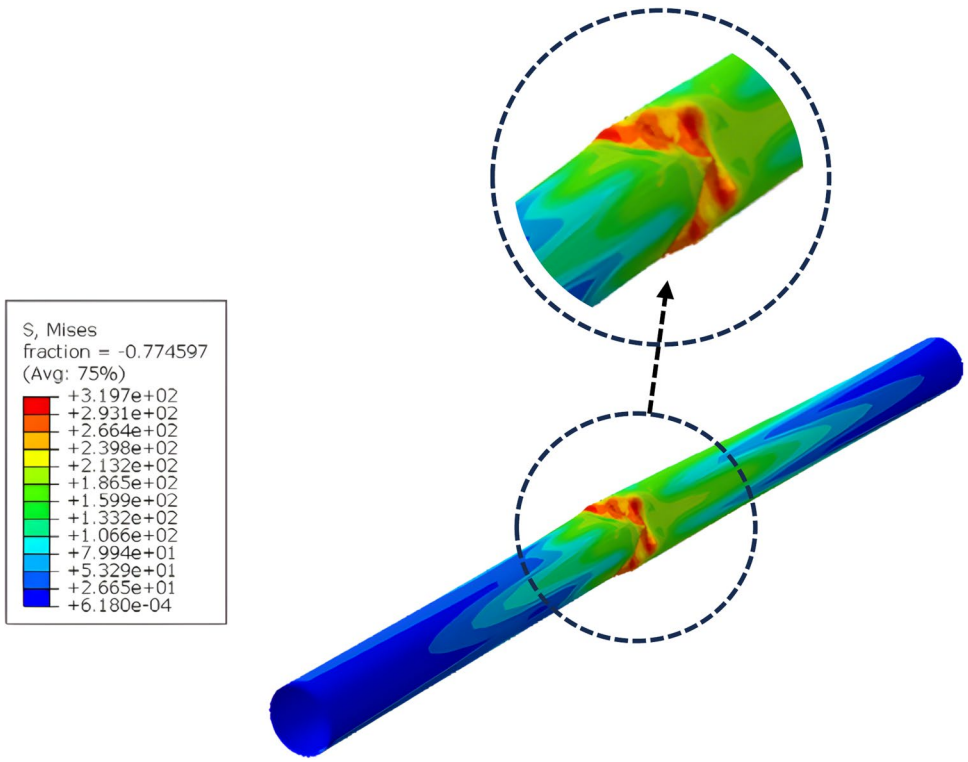

Fig. 21 Numerical analysis result of DT200-F (previous study)

deformation more realistically, in line with the observations made in the experiment.

For the DT171-F specimen, both results confirm the same overall deformation at the mid-span; however, the present result provides a sharper representation of the buckling pattern. A notable feature is that in the present result, the left side of the tube, from the edge to the local buckling zone, is slightly lifted higher than the right side. This asymmetrical deformation is consistent with the experimental observation, which also showed a similar upward inclination.

Overall, the comparison reveals that both the previous and present studies identify the same failure modes; however, the present analysis provides a clearer picture of the deformation. The buckling folds look sharper, the wave shapes are more visible, and the small asymmetrical lift is

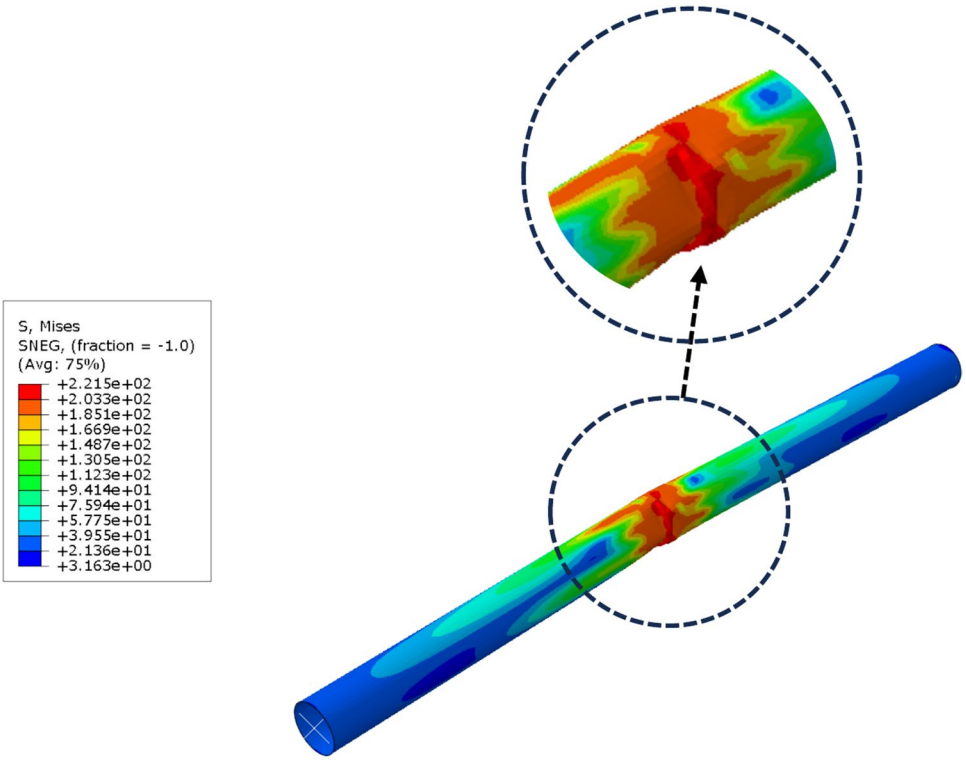

Fig. 22 Numerical analysis result of DT200-F (present study)

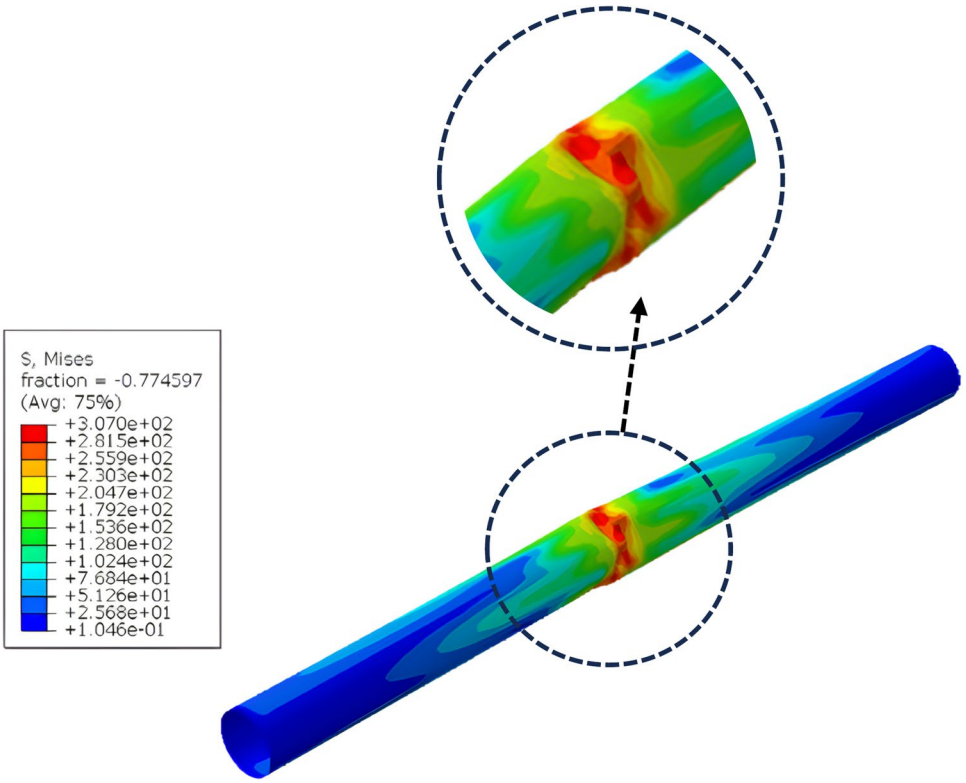

Fig. 23 Numerical analysis result of DT171-F (previous study)

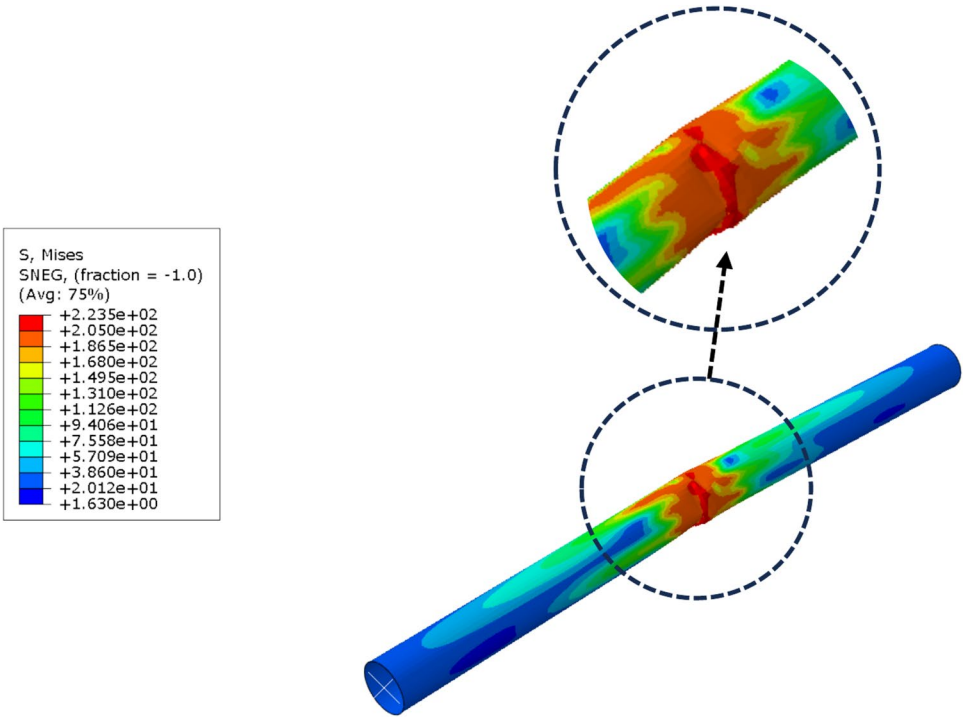

Fig. 24 Numerical analysis result of DT171-F (present study)

Table 7 Margin of error between the previous and present studies

Specimens label	Result			Error	
	Axial load of the experiment (kN)	Axial load of FEA in previous study (kN)	Axial load of FEA in the present study (kN)	Previous research	Present research
DT240-F	26	26.8	26.54829	2.98%	2.11%
DT200-F	36	34.72	36.83391	3.55%	2.32%
DT171-F	37	37.5	39.70849	1.33%	7.32%

also captured. These details make the present study more closely aligned with the observations from the experiment.

6 Results of the parametric study

6.1 Effect of load eccentric imperfection

In this sub-section, nonlinear static Riks analysis was performed for all geometries (DT240-F, DT200-F, and DT171-F) to assess the effect of load eccentricity. This method accounts for geometric nonlinearity and captures the post-buckling response under various eccentricity levels. The analysis provides insights into how increasing eccentricity affects both the ultimate load capacity and the buckling deformation pattern. The test variations were done by inputting different load eccentricities into three geometries, DT240-F, DT200-F, and DT171-F. There are five different magnitudes of load eccentricity on this variation: 0.005D, 0.01D, 0.02D, 0.04D, and 0.08D, where every magnitude is multiplied by the diameter of the cylindrical shell. The analysis results reveal that load eccentricity has a significant impact on the buckling behavior of structural elements subjected to axial loading [29].

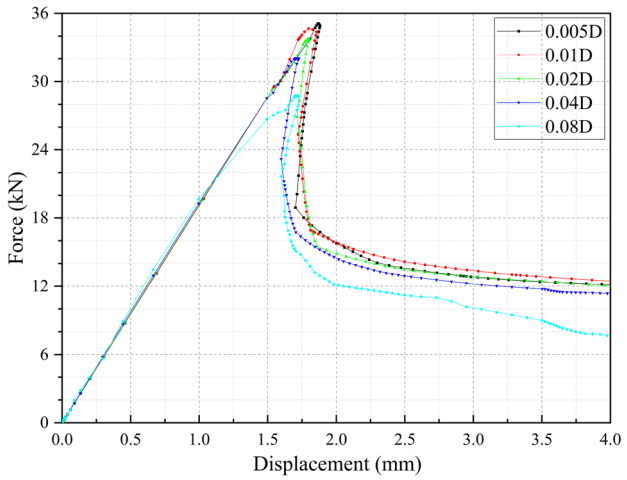

Fig. 25 Ultimate load graph of load eccentricity imperfection DT240-F

As shown in Figs. 25, 26, 27, the graph exhibits a downward trend as the load position becomes more eccentric. Figure 25 shows that the eccentric position of 0.005D in

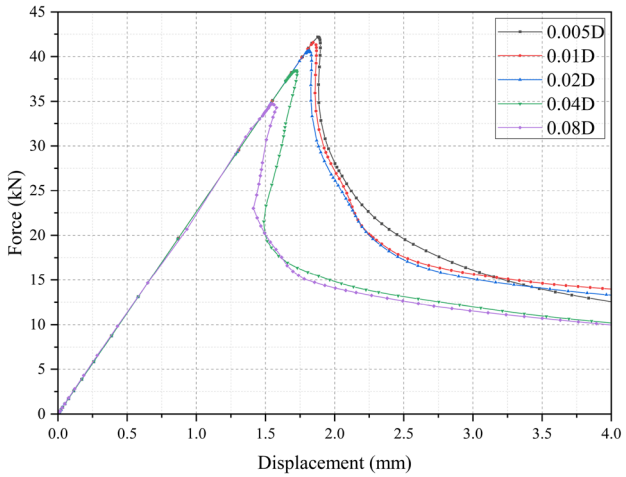

Fig. 26 Ultimate load graph of load eccentricity imperfection DT200-F

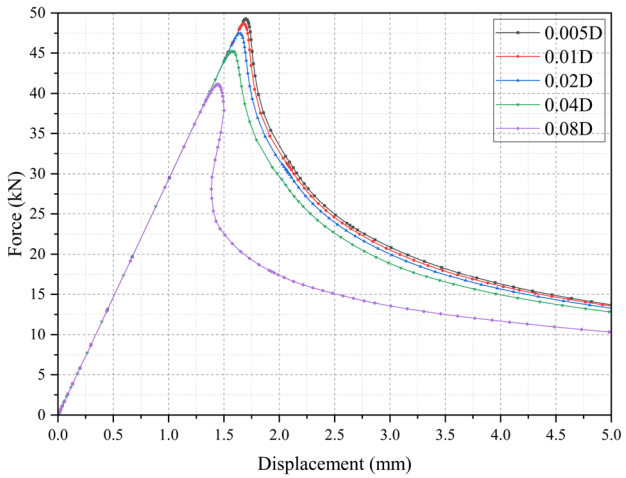

Fig. 27 Ultimate load graph of load eccentricity imperfection DT171-F

Table 8 Ultimate load of load eccentricity imperfection

Specimens label	Ultimate load (kN)				
	0.005D	0.01D	0.02D	0.04D	0.08D
DT240-F	35.12	34.66	33.74	32.05	28.76
DT200-F	42.19	41.57	40.62	38.46	34.72
DT171-F	49.29	48.70	47.46	45.25	41.13

the geometry of DT240-F has the highest ultimate load of 35.12 kN, followed by the more eccentric position of 0.08D, which shows that the ultimate load reached 28.76 kN. Then, in Fig. 26, the geometry of the DT200-F is demonstrated. The position of the more concentric load is 0.005D, and the highest ultimate load is achieved at 42.19 kN. At the more eccentric position, which is 0.08D, the ultimate load is achieved at 34.72 kN. The same phenomenon also occurs in Fig. 27, where the geometry of the DT171-F is depicted. The ultimate load is reached at a 0.005D position, corresponding to 49.29 kN. At a more eccentric position, the ultimate load is reached at 41.13 kN (see Table 8). This imperfection not only affects the structure's ability to resist axial compression, but it can also impact the shape and point of deformation that occur in the cylindrical shell. As shown in Figs. 28, 29, 30, the point of deformation shifts as the load position becomes more eccentric. It is shown that when the load is applied in a perfectly concentric position, the structural member demonstrates a higher critical buckling load; this holds for all geometries. However, as the eccentricity of the load increases, the critical buckling load decreases [30]. This behavior can be attributed to the additional bending moment introduced due to eccentricity. When the load is applied off-center, it generates a non-uniform stress distribution, combining axial compression with bending stresses. This causes premature local instability and asymmetric deformation, effectively reducing the shell's ability to carry compressive loads efficiently. This behavioral pattern is also observed in other research studies related to cylindrical shells under bending moments, such as those by Wang and Zhou [31], Yun et al. [32], and Adie et al. [33].

6.2 Effect of initial geometric imperfection

This subsection employs nonlinear geometric analysis, utilizing the Riks method, to investigate the influence of initial geometric imperfections on buckling strength. Only two geometries, DT240-F and DT171-F, are analyzed. The imperfections were introduced based on the first eigenmode shape obtained from a preceding linear buckling analysis and scaled accordingly. This ensures that both pre-buckling and post-buckling behaviors are captured in the nonlinear domain. Table 9 presents the results of the ultimate load from the numerical analysis, showing a downward trend in each variation. As shown in Fig. 31, the simulation results obtained at the 0.2t variation yield the highest ultimate load among the other variations in geometry, which is 35.55 kN. As the greater the variation is applied, the ultimate load decreases respectively, reaching a variation of 0.8t, where the ultimate load achieved is 35.28 kN. The same phenomenon is illustrated in Fig. 32, which depicts the geometry of the DT171-F. At the 0.2t variation, the ultimate load was reached at 49.69 kN, then decreased. At the 0.8t variation, the ultimate load point was reached at 47.47 kN. In the geometry of the DT240-F, the trend of the ultimate load decrease is not so significant due to the smaller thickness of the cylindrical shell compared to the geometry of the DT171-F, where the wall thickness of the cylindrical shell can also affect the strength of this structure in withstanding the given axial compression load. Additionally, this imperfection can also affect the position where the deformation occurs, as illustrated in Figs. 33 and 34. In the DT240-F geometry, most of the deformation occurs at the center point of the cylindrical shell, and the deformation point in the

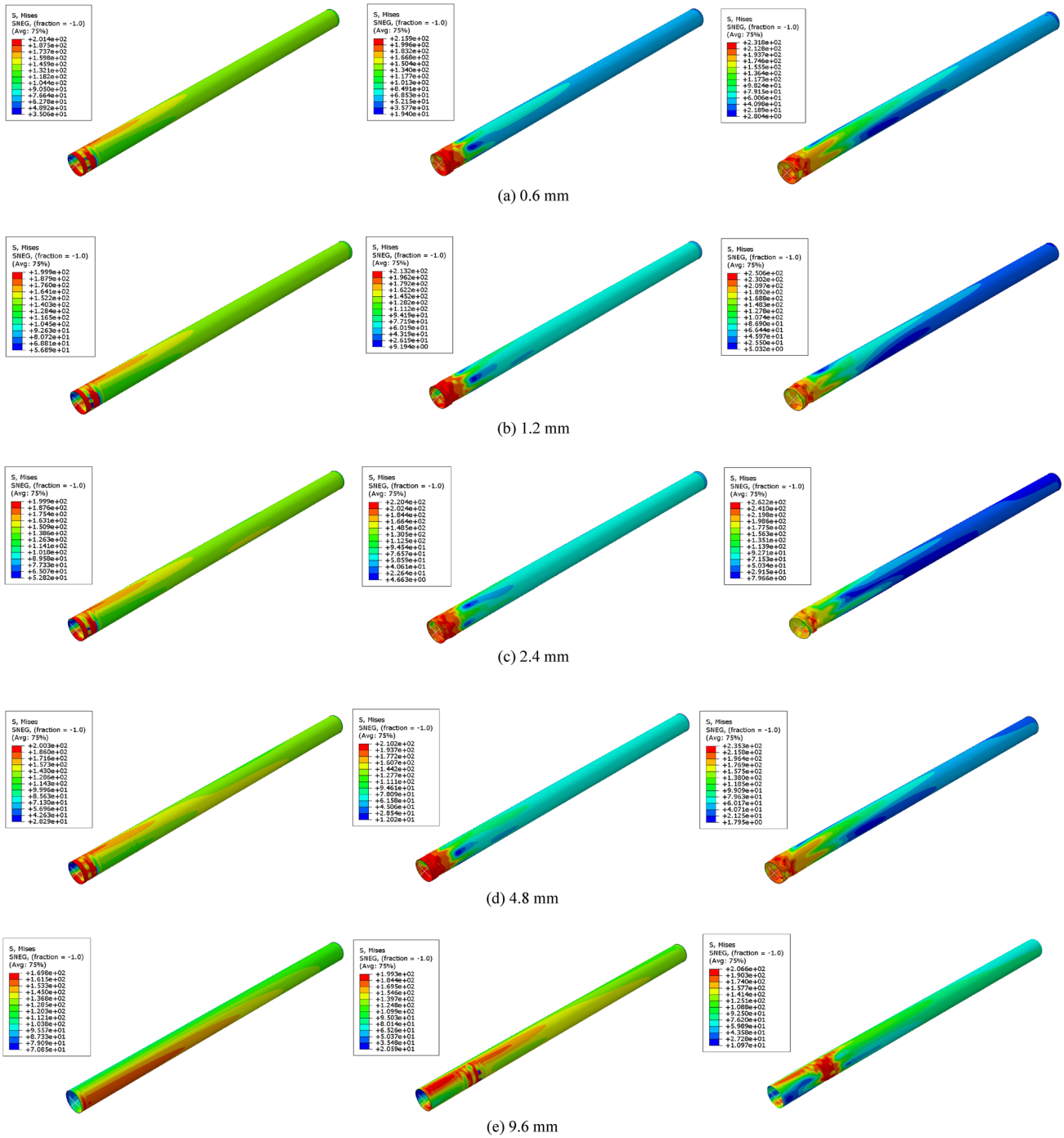

Fig. 28 Deformation results of load eccentricity imperfection DT240-F (**a**) 0.6 mm, (**b**) 1.2 mm (**c**) 2.4 mm, (**d**) 4.8 mm, (**e**) 9.6 mm

DT171-F geometry moves closer to the point where the load is applied. These imperfections serve as stress concentration initiators, reducing the effective stiffness and triggering local instability before the ideal buckling load is reached. They disturb the load path and break the structural symmetry, thereby increasing the susceptibility to early-mode buckling. Additionally, the higher wall thickness in DT171-F amplifies the sensitivity, showing greater degradation in performance compared to the thinner DT240-F, where the load drop is less pronounced. This indicates that thicker shells may not always be more robust if imperfections are present. Similar works related to imperfection and pipe thickness on pipes are noted in Balakrishnan et al. [34], Widiyanto et al. [35], and Srikanth and Michael [36].

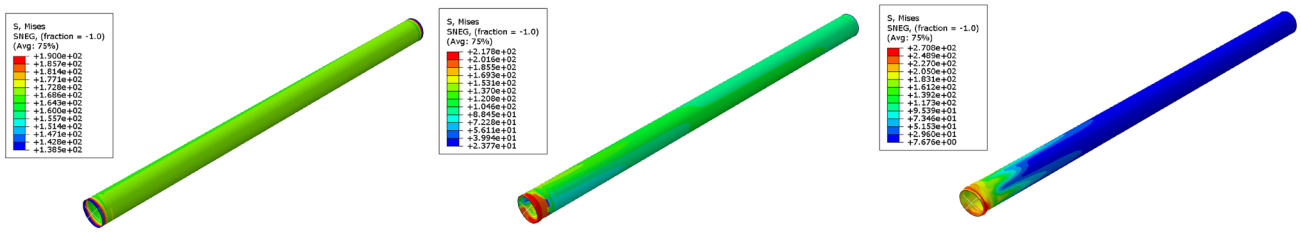

(a) 0.6 mm

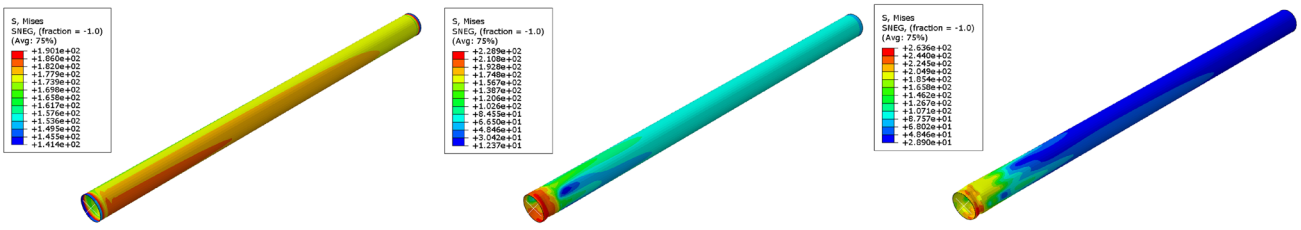

(b) 1.2 mm

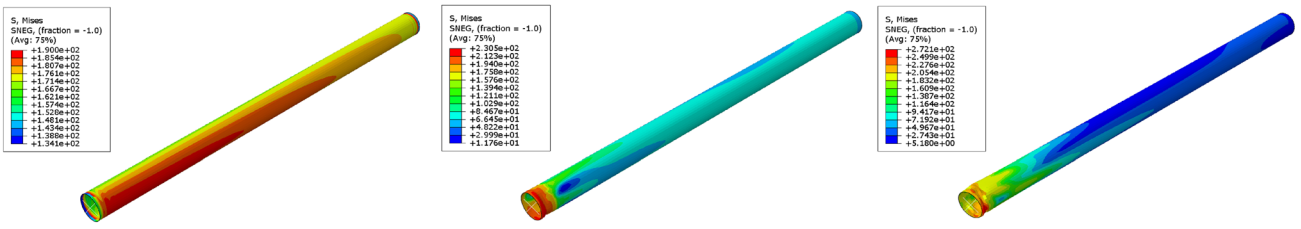

(c) 2.4 mm

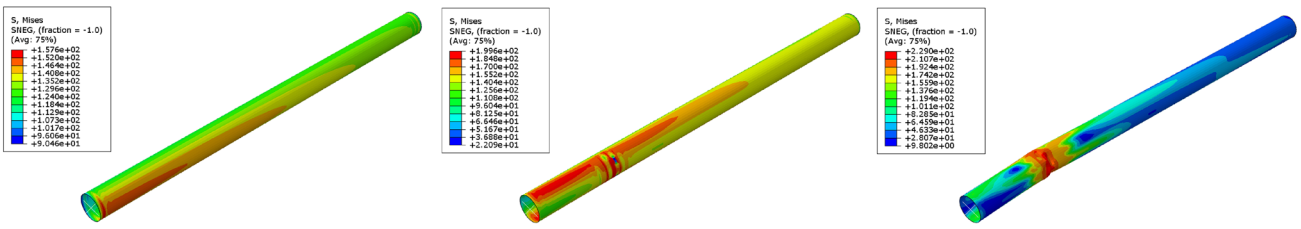

(d) 4.8 mm

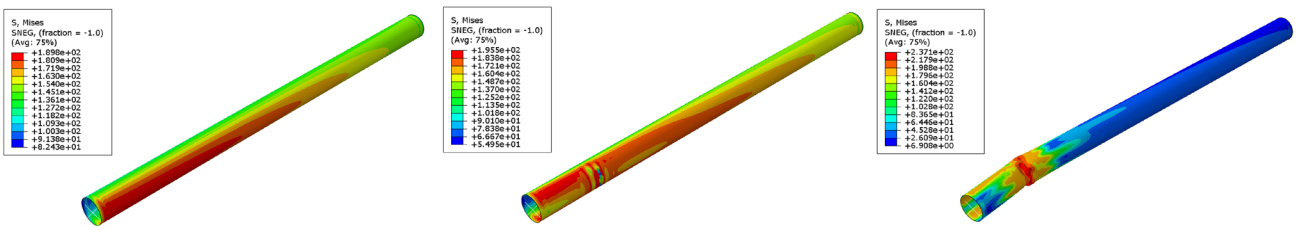

(e) 9.6 mm

Fig. 29 Deformation results of load eccentricity imperfection DT200-F (**a**) 0.6 mm, (**b**) 1.2 mm (**c**) 2.4 mm, (**d**) 4.8 mm, (**e**) 9.6 mm

6.3 Effect of longitudinal thickness imperfection

Nonlinear static Riks simulations were conducted for the DT240-F geometry to investigate the effect of longitudinal thickness imperfection. The analysis considered two variation schemes: alpha and beta, each introducing different types of thickness gradients along the shell length. The geometric nonlinearity is included to account for deformation localization and progressive collapse behavior caused by non-uniform shell thickness. Table 10 illustrates the variation in alpha applied to the geometry, indicating a trend of decreasing ultimate load and wall thickness in the cylindrical shell. Thinner wall sections in the alpha variation

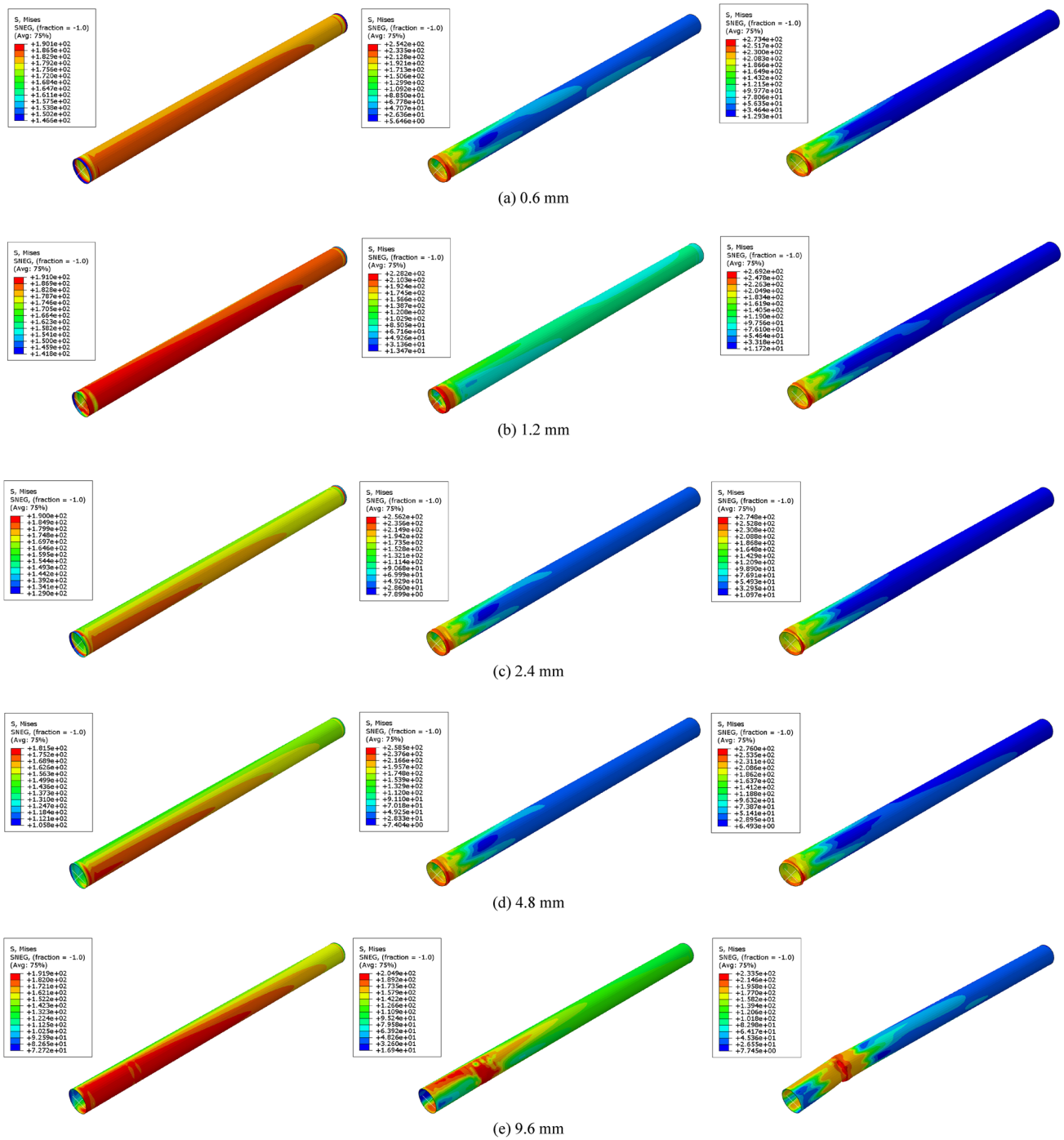

Fig. 30 Deformation results of load eccentricity imperfection DT171-F (**a**) 0.6 mm, (**b**) 1.2 mm (**c**) 2.4 mm, (**d**) 4.8 mm, (**e**) 9.6 mm

Table 9 Ultimate load of initial geometric imperfection

Specimens label	Ultimate load (kN)			
	0.2t	0.4t	0.6t	0.8t
DT240-F	35.55	35.54	35.42	35.28
DT171-F	49.46	48.79	48.10	47.47

resulted in reductions in ultimate load, primarily due to a localized reduction in shell stiffness that initiates local buckling zones and compromises global stability. In Fig. 35, the thickness variation 1 has the highest ultimate load, which was achieved at 20.78 kN with a final thickness of the cylindrical shell of 0.4 mm, and decreased as the thickness of the cylindrical shell decreased. The lowest ultimate load is

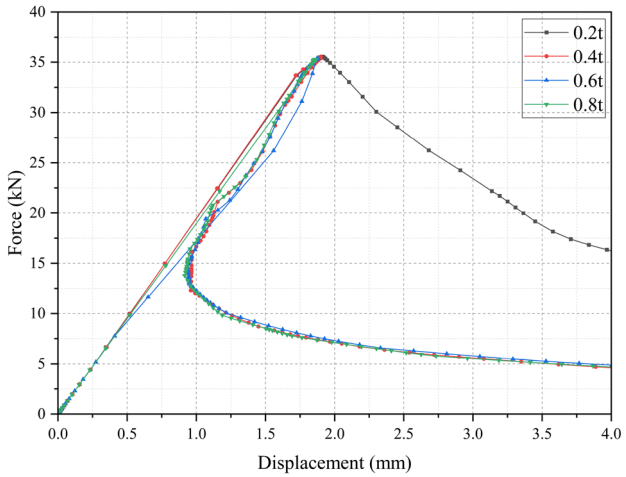

Fig. 31 Ultimate load graph of initial geometric imperfection DT240-F

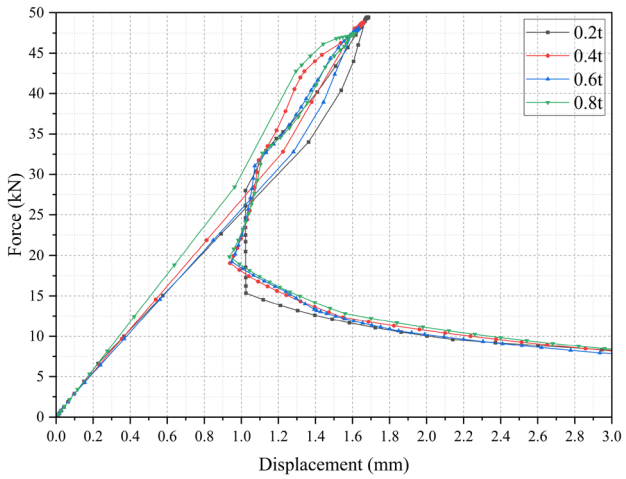

Fig. 32 Ultimate load graph of initial geometric imperfection DT171-F

observed at a thickness of 3, which is 18.49 kN with a final thickness of 0.36 mm.

Table 11 illustrates the beta variation applied to the geometry, exhibiting an increasing trend in the ultimate load. In Fig. 36, the thickness variation 4 shows that the ultimate load is reached at 20.78 kN, while it increases significantly to thickness 5, which has an ultimate load of 28.64 kN. Then, the increase in the ultimate load is insignificant when the thickness reaches 6, with the ultimate load at 28.66 kN. The lowest thickness of all variations is 0.4 mm, and thickness variation 4 has the lowest thickness at the end of the pipe where the load was applied. Then, thickness variation 5 has the lowest thickness point at the middle of the cylindrical shell, as does thickness variation 6, which has the two lowest thickness points in the right and left cylindrical shells. The result in Fig. 37 shows that the deformation form of the three variations tends to be the same, and deformation occurs at the end of the cylindrical shell with the thinnest thickness. However, a significant difference is observed in the form of deformation in the cylindrical shell, as shown in Fig. 38, where at a thickness of 4, deformation occurs near the location where the load was applied. Then, at a thickness of 5, deformation occurs at the central point of the cylindrical shell. At a thickness of 6, the deformation occurs at the point near where the load is applied. The beta variation demonstrated that altering the location of the thickness variation not only changed the buckling location but also affected the ultimate load. This underscores the critical role of imperfection positioning in determining not only when but also where buckling occurs. This pattern of buckling behaviors agrees with the pioneering findings by Karampour et al. [37], Liu and Wang [38], and Cai et al. [39].

7 Conclusions

The eccentricity of the load has a significant impact on the decrease in the ultimate load. The greater the eccentricity, the lower the ultimate load that can be achieved. This shows that the imperfection of load eccentricity is further away from the center point of the cylindrical shell. Then, at the initial geometric imperfections, the 0.2t to 0.8t variation in the DT240-F geometry exhibits a trend of insignificant decrease in ultimate load. This decrease is more pronounced in geometries with greater thickness, such as the DT171-F geometry. Therefore, the thickness of the cylindrical shell wall significantly affects the structure's stability in resisting axial compression loads with this imperfection. Then, the imperfection of the variation in thickness along the cylindrical shell (alpha and beta variations) impacts the ultimate load value and the location of buckling. In the alpha variation, the thinner the thickness of the cylindrical shell, the lower its strength in withstanding axial compression loads. Meanwhile, in the beta variation, the thickness distribution affects the buckling location but has an insignificant effect on the ultimate load. In this variation, the thickness of the pipe significantly affects the shape and point at which buckling occurs. It is also observed that, in some cases, while the deformation shape and stress distribution change significantly, the ultimate load remains relatively constant. This phenomenon can be attributed to the nature of the parameter, which affects only the post-buckling behavior without substantially altering the critical load path. For example, in the initial geometric imperfection variation of the DT240-F geometry, although the deformation shape shifts and stress localization occur differently with increasing imperfection amplitude (from 0.2t to 0.8t), the change in ultimate load is minimal. This is due to the relatively low wall thickness, which limits the structure's sensitivity to minor geometric deviations. Additionally, certain imperfection types (e.g., beta variation in thickness distribution) alter the location

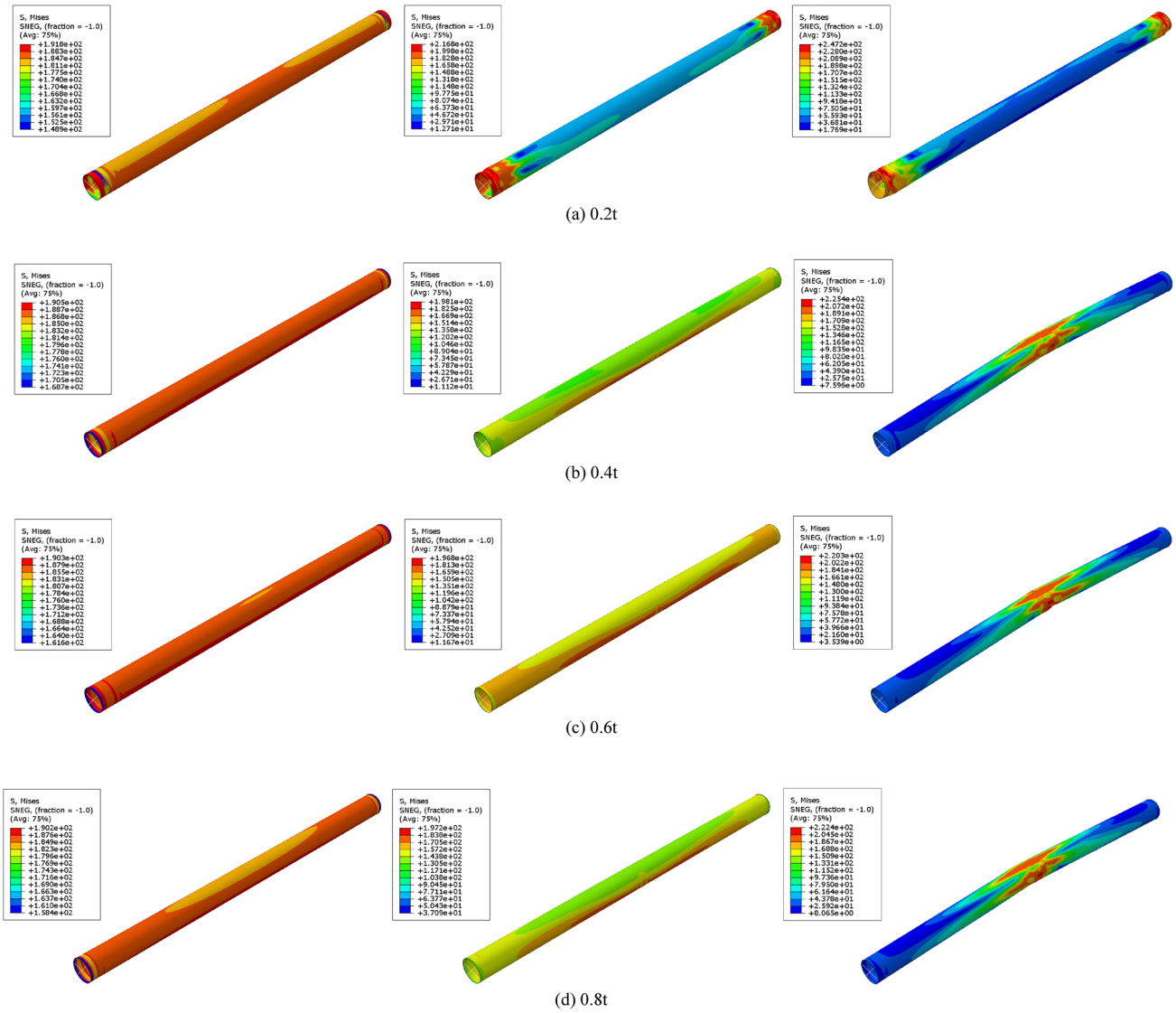

Fig. 33 Deformation results of initial geometric imperfection DT240-F (**a**) 0.2t, (**b**) 0.4t, (**c**) 0.6t, (**d**) 0.8t

of buckling but not the structural stiffness to a degree sufficient to reduce the peak load capacity. Therefore, while these imperfections influence the mode of deformation and stress patterns, their effect on the critical buckling strength is not always significant, particularly when the changes do not result in a considerable reduction in the effective cross-sectional area or overall stiffness, which significantly affects the stability of the structure in resisting axial compression loads in all geometries. Additionally, the shape and position of the deformation also change as the load is applied.

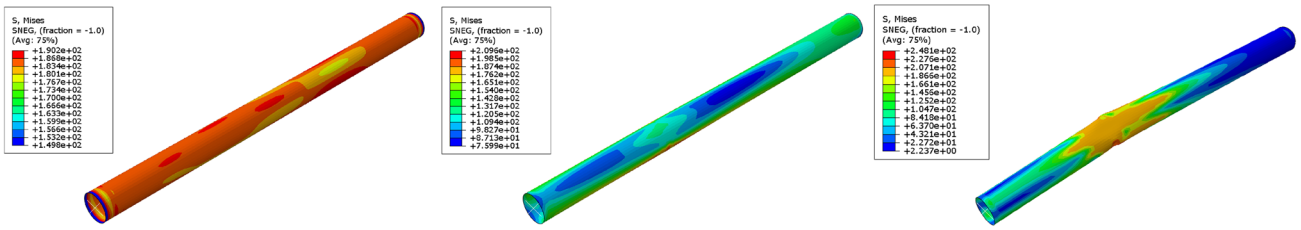

(a) 0.2t

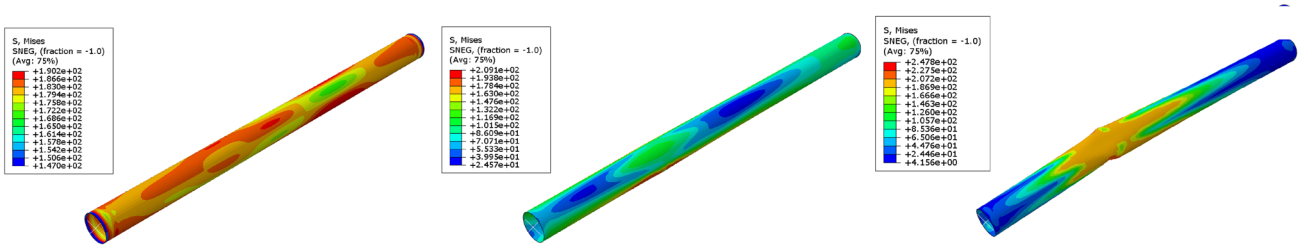

(b) 0.4t

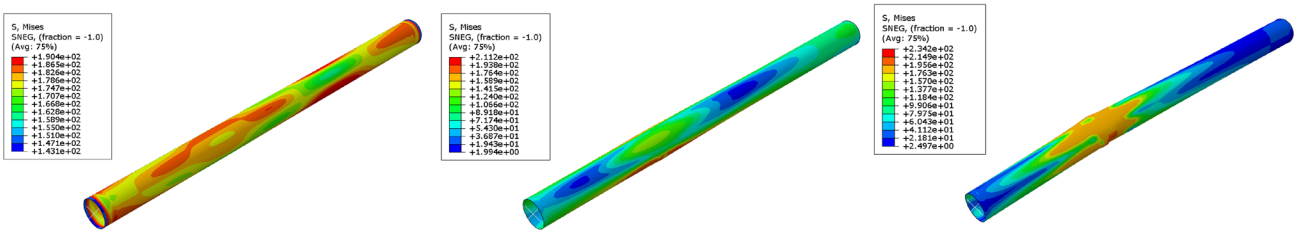

(c) 0.6t

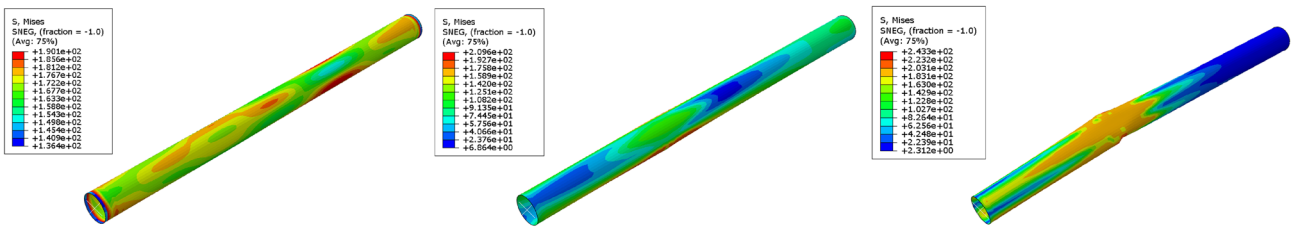

(d) 0.8t

Fig. 34 Deformation results of initial geometric imperfection DT171-F (**a**) 0.2t, (**b**) 0.4t (**c**) 0.6t, (**d**) 0.8t

Table 10 Ultimate load of longitudinal thickness imperfection (alpha variation)

Thickness number	Ultimate load (kN)
Thickness_1	20.78
Thickness_2	18.65
Thickness_3	18.49

Table 11 Ultimate load of longitudinal thickness imperfection (beta variation)

Thickness number	Ultimate load (kN)
Thickness_4	20.78
Thickness_5	28.64
Thickness_6	28.66

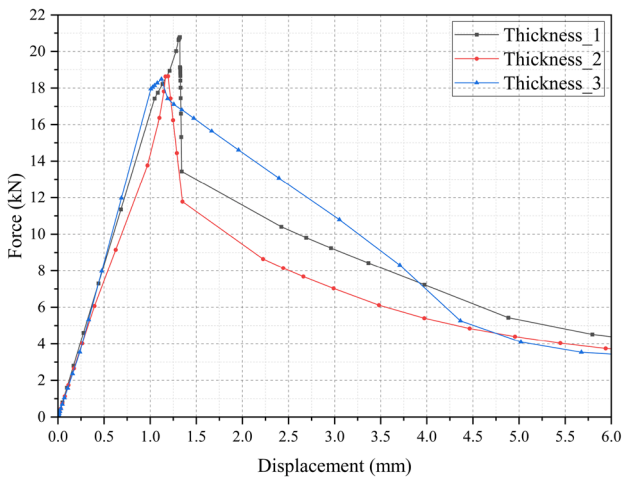

Fig. 35 Ultimate load graph of longitudinal thickness DT240-F (alpha variation)

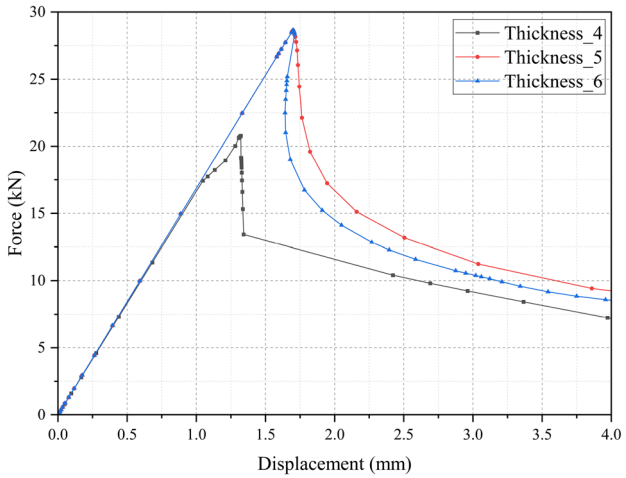

Fig. 36 Ultimate load graph of longitudinal thickness DT240-F (beta variation)

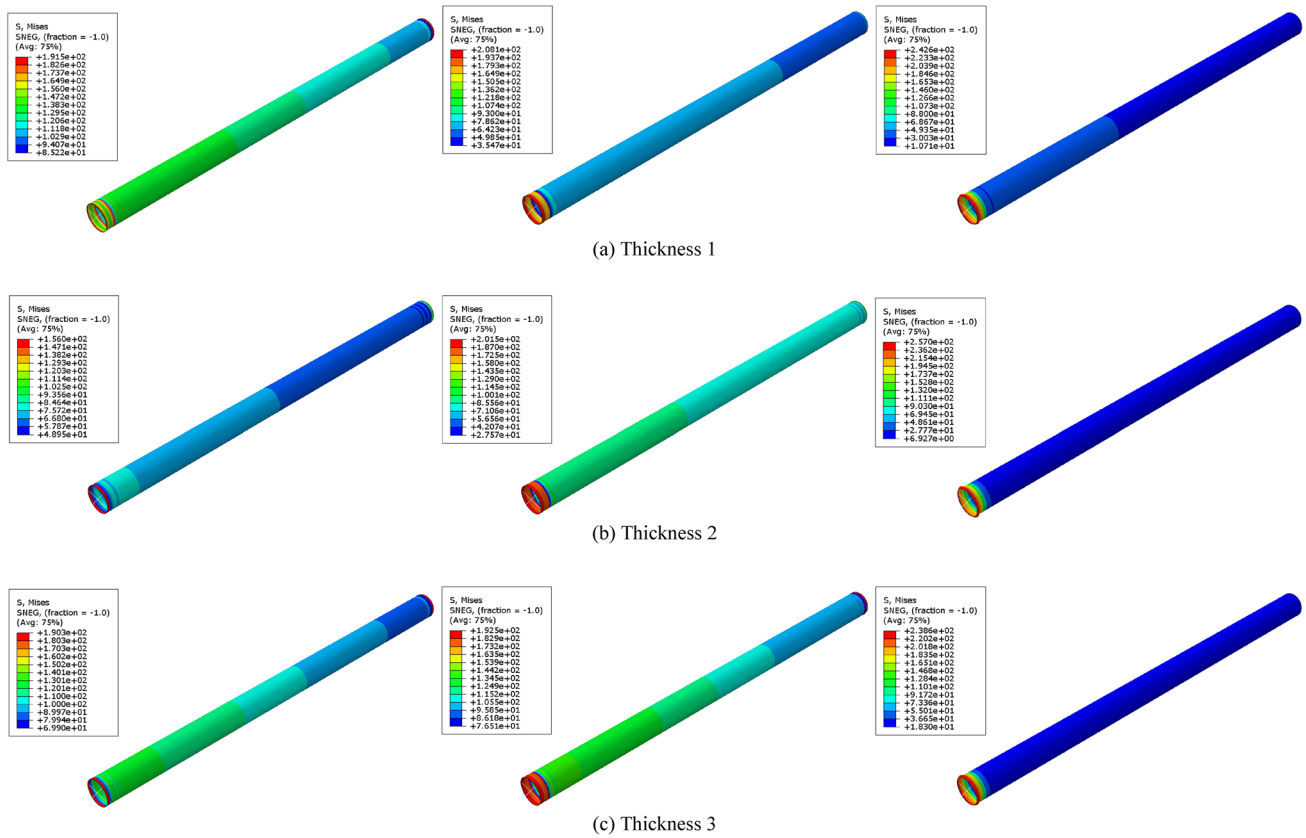

Fig. 37 Deformation results of longitudinal thickness imperfection DT240-F (alpha variation)

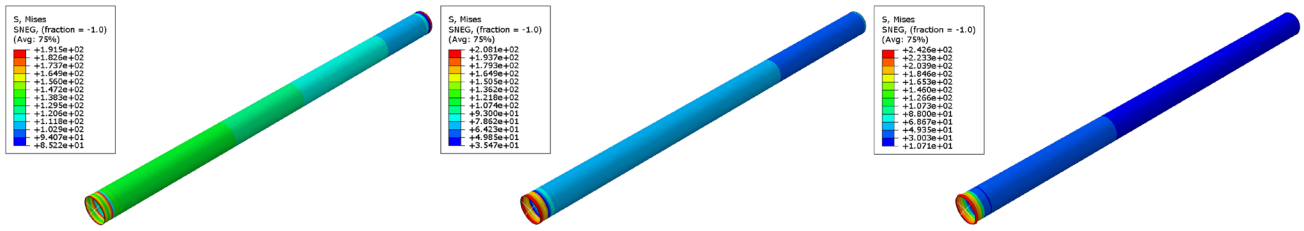

(a) Thickness 4

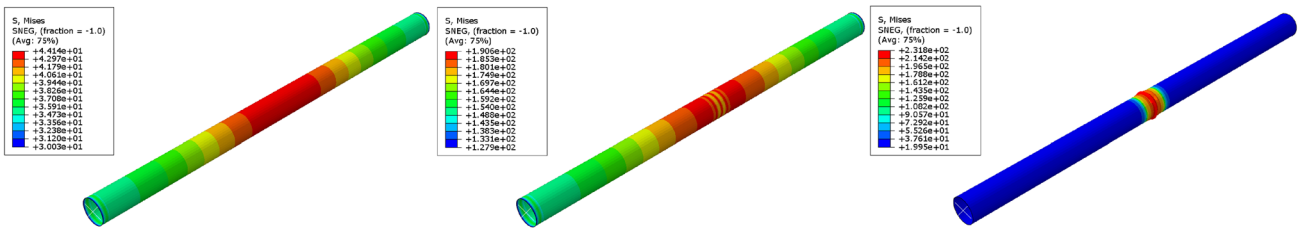

(b) Thickness 5

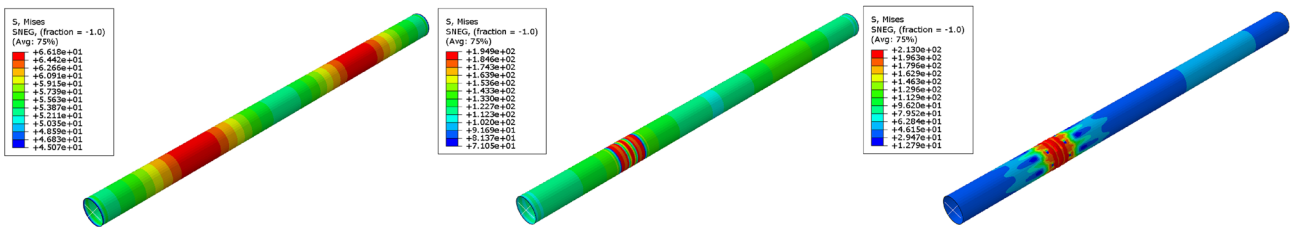

(c) Thickness 6

Fig. 38 Deformation results of longitudinal thickness imperfection DT240-F (beta variation)

Acknowledgements This work was supported by the RKAT PTNBH Universitas Sebelas Maret Year 2025, under the Research Scheme of "Penelitian Kolaborasi Internasional" (KI-UNS), with research grant/contract no. 369/UN27.22/PT.01.03/2025. The authors highly acknowledge this support.

Authors' contributions Aryanda Rakhmad Maharditya: Formal analysis, Investigation, Writing—Original Draft. Ben Ganendra: Writing—Original Draft, Software. Indri Yaningsih: Methodology, Project administration, Funding acquisition. Aditya Rio Prabowo: Validation, Writing—Review & Editing, Supervision, Project administration, Funding acquisition. Sören Ehlers: Writing—Review & Editing. Moritz Braun: Writing—Review & Editing. Quang Thang Do: Data Curation, Methodology. Wibowo Wibowo: Conceptualization, Supervision. Teguh Muttaqie: Conceptualization, Software, Visualization. Iwan Istanto: Conceptualization, Funding acquisition. Rahman Wijaya: Visualization, Funding acquisition.

Funding Universitas Sebelas Maret, 369/UN27.22/PT.01.03/2025, Indri Yaningsih.

Availability of data and materials The authors confirm that the data supporting the findings of this study are available within the article.

Declarations

Competing interest The authors declare that they have no competing interests.

References

1. Kamarudin MNB, Ali JSM, Aabid A, Ibrahim YE (2022) Buckling analysis of a thin-walled structure using finite element method and design of experiments. Aerospace 9:541. https://doi.org/10.3390/aerospace9100541
2. Lee JH, Oh YC, Seo KC (2017) Development of design formula for predicting post-buckling behaviour and ultimate strength of cylindrical shell". J Korean Soc Mar Environ Saf 23:313–319. https://doi.org/10.7837/kosomes.2017.23.3.313
3. Ganendra B, Prabowo AR, Muttaqie T, Adiputra R, Ridwan R, Fajri A, Do QT, Carvalho H, Baek SJ (2023) Thin-walled cylindrical shells in engineering designs and critical infrastructures: a systematic review based on the loading response. Curved and Layered Structures 10:20220202. https://doi.org/10.1515/cls-2022-0202

4. Teng JG, Rotter JM (2010) Cylindrical shells under axial compression - in Buckling of Thin Metal Shells. Spon Press, London, UK. https://doi.org/10.4324/9780203301609_chapter_2
5. Pan X, Zhao W, Chen L, Liu T, Deng J, Zhang Y, Zhu S, Li W (2024) Experimental investigation on axial quasi-static compression and low-velocity impact behaviors of perforated thermoplastic composite cylindrical shells. Compos Struct 343:118311. https://doi.org/10.1016/j.compstruct.2024.118311
6. Mandal P, Calladine CR (2000) Buckling of thin cylindrical shells under axial compression. Int J Solids Struct 37:4509–4525. https://doi.org/10.1016/S0020-7683(99)00160-2
7. Lundquist EE (1933) Strength tests of thin-walled duralumin cylinders in compression, Langley Memorial Aeronautical Laboratory , Virginia, US.
8. Ma H, Jiao P, Li H, Cheng Z, Chen Z (2023) Buckling analyses of thin-walled cylindrical shells subjected to multi-region localized axial compression: experimental and numerical study. Thin-Walled Struct 183:110330. https://doi.org/10.1016/J.TWS.2022.110330
9. Kainat M, Cheng JJR, Martens M, Adeeb S (2015) Measurement and characterization of the initial geometric imperfections in high strength U-ing, O-ing and expanding manufactured steel pipes. J Press Vessel Technol Trans ASME 138(2):021201. https://doi.org/10.1115/1.4031507
10. Priyadarsini RS, Kalyanaraman V, Srinivasan SM (2012) Numerical and experimental study of buckling of advanced fiber composite cylinders under axial compression. Int J Struct Stab Dyn 12(4):12500289. https://doi.org/10.1142/S0219455412500289
11. Badamchi K, Showkati H (2022) Experiments on buckling behavior of thin-walled steel pipes subjected to axial compression and external pressure. Thin-Walled Struct 174:109122. https://doi.org/10.1016/j.tws.2022.109122
12. Huang H, Han Q (2008) Buckling of imperfect functionally graded cylindrical shells under axial compression. Eur J Mech A/Solids 27(6):1026–1036. https://doi.org/10.1016/j.euromechsol.2008.01.004
13. Ullah H (2009) Buckling of thin-walled cylindrical shells under axial compression. Int J Numer Method Eng 79(11):1332–1353. https://doi.org/10.1002/nme.2612
14. Yu C, Chen Z, Wang J, Yan S, Yang L (2012) Effect of welding residual stress on plastic buckling of axially compressed cylindrical shells with patterned welds. Proc Inst Mech Eng Part C J Mech Eng Sci 226(1):2381–2392. https://doi.org/10.1177/0954406211433976
15. Cao G, Chen Z, Yang L, Fan H, Zhou F (2015) Analytical study on the buckling of cylindrical shells with arbitrary thickness imperfections under axial compression. J Press Vessel Technol Trans ASME 137(1):041301. https://doi.org/10.1115/1.4027179
16. Ifayefunmi O (2016) Buckling behavior of axially compressed cylindrical shells: comparison of theoretical and experimental data. Thin-Walled Struct 98:558–564. https://doi.org/10.1016/j.tws.2015.10.027
17. Chen Z, Fan H, Cheng J, Jiao P, Xu F, Zheng C (2018) Buckling of cylindrical shells with measured settlement under axial compression". Thin-Walled Struct 123:351–359. https://doi.org/10.1016/j.tws.2017.11.006
18. Tu S, Shuai J (2020) Numerical study on the buckling of pressurized pipe under eccentric axial compression. Thin-Walled Struct 147:106542. https://doi.org/10.1016/j.tws.2019.106542
19. Eglītis E, Kalniņš K, Ozoliņš O (2010) Experimental and numerical study on buckling of axially compressed composite cylinders. Sci J Riga Tech Univ Constr Sci. https://doi.org/10.2478/v10137-009-0004-2
20. Wang B, Du K, Hao P, Tian K, Chao YJ, Jiang L, Xu S, Zhang X (2019) Experimental validation of cylindrical shells under axial compression for improved knockdown factors. Int J Solids Struct 164:37–51. https://doi.org/10.1016/j.ijsolstr.2019.01.001
21. Timoshenko SP, Gere JM, Prager W (1962) Theory of Elastic Stability. Courier Corporation, Massachusetts, United States
22. Wibawa LAN (2020) Numerical study of the effect of wall thickness and internal pressure on Von Mises stress and safety factor of thin-walled cylinder for rocket motor case. Jurnal Sains dan Teknologi 9(1):30–38. https://doi.org/10.23887/jst-undiksha.v9i1.24484
23. Matvienko Y (2013) Safety factors in structural integrity assessment of components with defects. Int J Struct Integr 4(4):457–476. https://doi.org/10.1108/IJSI-09-2012-0022
24. Bardi FC, Kyriakides S (2006) Plastic buckling of circular tubes under axial compression-part I: Experiments. Int J Mech Sci 48(8):830–841. https://doi.org/10.1016/j.ijmecsci.2006.03.005
25. Hallai JF, Kyriakides S (2011) On the effect of Lüders bands on the bending of steel tubes. Part I: experiments. Int J Solids Struct 48:3275–3284. https://doi.org/10.1016/j.ijsolstr.2011.06.024
26. Guo L, Yang S, Jiao H (2013) Behavior of thin-walled circular hollow section tubes subjected to bending. Thin-Walled Struct 73:281–289. https://doi.org/10.1016/j.tws.2013.08.014
27. Bracamonte AJ, Puche VM, Arguelles GM, Pumarejo LF, Ortiz AR, Herazo LCS (2023) Effect of Finite Element Method (FEM) Mesh Size on the Estimation of Concrete Stress-Strain Parameters. Appl Sci 13(4):2352. https://doi.org/10.3390/app13042352
28. Krasovsky V, Marchenko V, Schmidt R (2011) Deformation and buckling of axially compressed cylindrical shells with local loads in numerical simulation and experiments. Thin-Walled Struct 49(5):576–580. https://doi.org/10.1016/j.tws.2010.09.009
29. Zarei MJ, Hatami S, Azandariani MG, Gholami M (2024) Investigation of the mechanical performance of the sandwich cylindrical shell with a truss core under eccentric loading. Struct 61:105963. https://doi.org/10.1016/j.istruc.2024.105963
30. Wysmulski P, Debski H, Falkowicz K (2022) Sensitivity of compressed composite channel columns to eccentric loading. Mat 15(19):6938. https://doi.org/10.3390/ma15196938
31. Wang Q, Zhou W (2021) Burst capacity analysis of thin-walled pipe elbows under combined internal pressure and bending moment. Int J Press Vessel Piping 194:104652. https://doi.org/10.1016/j.ijpvp.2021.104562
32. Yun SH, Koo YD, Na MG (2020) Collapse moment estimation for wall-thinned pipe bends and elbows using deep fuzzy neural networks. Nucl Eng Technol 52(11):2678–2685
33. Adie PW, Adiputra R, Prabowo AR, Erwandi E, Muttaqie T, Muhayat N, Huda N (2023) Assessment of the OTEC cold water pipe design under bending loading: a benchmarking and parametric study using finite element approach. J Mech Behav Mat 32(1):20220298. https://doi.org/10.1515/jmbm-2022-0298
34. Balakrishnan S, Veerappan AR, Shanmugam S (2021) Development of a new improved structural integrity assessment correlation for throughwall axially cracked 90° shape imperfect pipe bends under in-plane opening bending moment. Int J Pres Vessel Piping 194:104526. https://doi.org/10.1016/j.ijpvp.2021.104526
35. Widiyanto I, Muttaqie T, Prabowo AR, Hadi S, Yaningsih I, Laksono FB (2022) Numerical analysis of stiffened offshore pipe subjected to environmental loading: a study case using external pressure. Proc Struct Integr 41:274–281. https://doi.org/10.1016/j.prostr.2022.05.032
36. Srikanth K, Michael TC (2024) Effect of shape-imperfections on fatigue life of elbows under in-plane cyclic loading. Alexandria Eng J 97:33–43. https://doi.org/10.1016/j.aej.2024.03.110
37. Karampour H (2018) Effect of proximity of imperfections on buckle interaction in deep subsea pipelines. Mar Strcut 59:444–457. https://doi.org/10.1016/j.marstruc.2018.02.011

38. Liu R, Wang X (2018) Lateral global buckling high-order mode analysis of a submarine pipeline with imperfection. Appl Ocean Res 73:107–126. https://doi.org/10.1016/j.apor.2018.01.014
39. Cai J, Jiang X, Lodewijks G, Pei Z, Wu W (2018) Residual ultimate strength of seamless metallic pipelines under a bending moment-a numerical investigation. Ocean Eng 164:148–159. https://doi.org/10.1016/j.oceaneng.2018.06.044